

# Pion physics with dressed quark-gluon vertices

M.N. Ferreira,<sup>1,2,\*</sup> A.S. Miramontes,<sup>3,†</sup> J.M. Morgado,<sup>3,‡</sup>

J. Papavassiliou,<sup>3,§</sup> and J.M. Pawłowski<sup>4,5,¶</sup>

<sup>1</sup>*School of Physics, Nanjing University, Nanjing, Jiangsu 210093, China*

<sup>2</sup>*Institute for Nonperturbative Physics,*

*Nanjing University, Nanjing, Jiangsu 210093, China*

<sup>3</sup>*Department of Theoretical Physics and IFIC, University of Valencia and CSIC,*

*E-46100, Valencia, Spain*

<sup>4</sup>*Institut für Theoretische Physik, Universität Heidelberg,*

*Philosophenweg 16, Heidelberg, 69120, Germany*

<sup>5</sup>*ExtreMe Matter Institute EMMI, GSI, Planckstrasse 1, Darmstadt, 64291, Germany*

## Abstract

Recently, a theoretical framework was set up in [1], which allows for the symmetry-preserving inclusion of full quark-gluon vertices in the description of the meson dynamics. In the present work, we develop a special truncation within this approach, which leads to a tractable set of functional equations that satisfy the fundamental chiral Ward-Takahashi identities. Specifically, the truncation allows us to simplify considerably the quark-gluon Schwinger-Dyson equation, without significant loss of quantitative accuracy. Importantly, this implies a substantial reduction of complexity of the renormalized Bethe-Salpeter equation: it is composed by a pair of one-loop diagrams that contain the full quark-gluon vertex, and a single two-loop diagram that is instrumental for the masslessness of the pion in the chiral limit. A detailed numerical analysis reveals that the incorporation of the aforementioned two-loop diagram is instrumental for the corresponding eigenvalue to reach unity. The key relation between the quark mass function and the pion wave function is shown to be satisfied to within the numerical precision of the loop integrals, which is at the level of about one percent or better. The field-theoretic ingredients required for the extension of this analysis beyond the chiral limit are briefly discussed.

---

\* [mnferreira@nju.edu.cn](mailto:mnferreira@nju.edu.cn)

† [angel.s.miramontes@uv.es](mailto:angel.s.miramontes@uv.es)

‡ [jose.m.morgado@uv.es](mailto:jose.m.morgado@uv.es)

§ [joannis.papavassiliou@uv.es](mailto:joannis.papavassiliou@uv.es)

¶ [j.pawlowski@thphys.uni-heidelberg.de](mailto:j.pawlowski@thphys.uni-heidelberg.de)

## I. INTRODUCTION

The self-consistent incorporation of QCD correlation functions into the dynamical equations that govern the physics of hadrons is particularly challenging, requiring the development of sophisticated truncation schemes, see, *e.g.*, [2–23]. Recently, a theoretical framework was developed, which allows for the self-consistent inclusion of non-trivial quark-gluon vertices in the dynamical equations describing the physics of mesons [1]. In particular, the set of Schwinger-Dyson equations (SDEs) satisfied by the quark propagator,  $S$ , the quark-gluon vertex,  $\Gamma^\mu$ , and the (non-singlet) axial-vector vertex,  $\Gamma_5^\mu$ , [24–34] are completely compatible with the constraints imposed by the chiral symmetry, in the form of Ward-Takahashi identities (WTIs).

The analysis of [1] singles out a practically unexplored correlation function [7, 35], denominated “gluon-axial-vector vertex”, and denoted by  $G_5^{\mu\nu}$ . The rôle of this vertex is instrumental, because its inclusion in the SDE of  $\Gamma_5^\mu$  allows for a symmetry-preserving departure from the confines of the rainbow-ladder (RL) approximation [36–58]. Note that the symmetry-restoring action of  $G_5^{\mu\nu}$  hinges on the WTI that connects it to the quark-gluon vertex  $\Gamma^\mu$ . However, as illustrated in [1], the dynamical equation that determines  $G_5^{\mu\nu}$  has a rather complicated structure, being composed by graphs that contain  $G_5^{\mu\nu}$  explicitly (“*G-dependent*”), and those containing  $\Gamma_5^\mu$  instead (“*G-independent*”). Therefore, a truncation that reduces the complexity of this equation without compromising its symmetry properties would be particularly useful, allowing for a preliminary numerical exploration of this novel approach.

In the present work we show that such a truncation is indeed feasible, as long as the corresponding quark-gluon vertices are also appropriately modified. In particular, one may drop the *G*-dependent diagrams entirely, by setting  $G_5^{\mu\nu} = 0$  inside them, such that the gluon-axial-vector vertex is exclusively computed from the *G*-independent graphs. The symmetry remains intact (*i.e.*, the key WTIs are still satisfied) provided that, at the same time, a simplified version of the SDE that governs the quark-gluon vertex is used [12, 59, 60]. In particular, denoting by  $q$  the momentum of the gluon, one sets  $\Gamma^\mu(q, r, -p) = V(q)\gamma^\mu$  *inside* the relevant diagrams, where the function  $V(q)$  corresponds to the classical form factor of the quark-gluon vertex in the so-called “symmetric” kinematic configuration defined as  $q^2 = r^2 = p^2$ .

We stress that, although the aforementioned SDE takes  $V(q)$  as input, it returns a quark-gluon vertex that displays the full kinematic content. It possesses eight transverse form factors, and in the Landau gauge the longitudinal ones do not take part in the dynamics. These form factors depend non-trivially on three kinematic variables. We also note, that a variant of this approximation has been used in the detailed study of the quark-gluon vertex presented in [61].

Within this truncation, the dynamical equation for  $G_5^{\mu\nu}$  is drastically simplified, and we readily obtain the Bethe-Salpeter equation (BSE) that controls the formation of the bound states (pions) [2, 62–66]. This BSE consists of four diagrams, one corresponding to the standard RL graph, but now with *dressed vertices*, and three additional graphs that originate precisely from the vertex  $G_5^{\mu\nu}$ . Once the multiplicative renormalization has been carried out, see [67–69], the final BSE is described by three diagrams, two that are “one-loop dressed” and one that is “two-loop dressed”. The full quark-gluon vertex enters both in the quark gap equation and the one-loop dressed diagrams of the BSE.

Importantly, the numerical solution of the BSE for massless pions in the chiral limit reveals that the dominant term of the pion amplitude satisfies the axial WTI [70, 71] within the numerical accuracy of the loop integrals, see Fig. 10.

The article is organized as follows. In Sec. II we review the theoretical framework, introducing the key quantities, together with the most salient relations. Next, in Sec. III, we discuss in detail the symmetry-preserving truncation of the dynamical equation satisfied by  $G_5^{\mu\nu}$ . In Sec. IV the truncation is employed to obtain the BSE that controls the formation of pions. In Sec. V the multiplicative renormalization of the SDE-BSE system is carried out. Then, in Sec. VI we solve the system to obtain the Bethe-Salpeter amplitude (BSA) of the massless pion. In Sec. VII we present our discussion and conclusions. Finally, in App. A we offer a diagrammatic demonstration of the WTI satisfied by the vertex  $G_5^{\mu\nu}$  within the truncation employed, while in App. B we discuss an interesting integral identity connecting the chirally symmetric and chiral symmetry breaking terms of the quark-gluon vertex.

## II. REVIEW OF THE THEORETICAL FRAMEWORK

In this section we present a brief account of the main ingredients, key relations, and general notation employed in the present work.

We start by pointing out that the calculations will be carried out in Minkowski space, and the final results will be passed to Euclidean space, in order to implement the numerical treatment. The main elements of our analysis may be summarized as follows.

(i) The central component of this approach is the axial-vector vertex,  $\Gamma_5^{a\mu} = t^a \Gamma_5^\mu$ , where  $t^a$  are the generators of the flavour  $SU(N_f)$  algebra; for  $N_f = 2$ ,  $t^a = \sigma^a/2$ , while for  $N_f = 3$ ,  $t^a = \lambda^a/2$ , where  $\sigma^a$  and  $\lambda^a$  are the Pauli and Gell-Mann matrices, respectively. Note that this vertex is associated with the flavour non-singlet current  $j_5^{a\mu}(x) = \bar{\psi}(x)\gamma_5\gamma^\mu t^a\psi(x)$ , see discussion in Appendix B of [1].

In the limit of vanishing current quark masses ( $m = 0$ ), the vertex  $\Gamma_5^\mu$  satisfies the well-known WTI [70, 72]

$$-P_\mu \Gamma_5^\mu(P, p_2, -p_1) = S^{-1}(p_1)\gamma_5 + \gamma_5 S^{-1}(p_2), \quad (2.1)$$

where  $S^{-1}(p)$  is the inverse quark propagator.

(ii) According to the usual decomposition,

$$S^{-1}(p) = A(p)\not{p} - B(p), \quad (2.2)$$

where  $A(p)$  and  $B(p)$  are the dressings of the (Dirac) vector and scalar structures, respectively, and  $\mathcal{M}(p) = B(p)/A(p)$  is the constituent quark mass.

The momentum evolution of  $A(p)$  and  $B(p)$  is controlled by the gap equation, shown in Fig. 1A, given by

$$S^{-1}(p) = \not{p} - m + ig^2 C_f \int_q \gamma^\nu S(q) \Gamma^\mu(q - p, p, -q) \Delta_{\mu\nu}(q - p), \quad (2.3)$$

which involves the fully-dressed quark-gluon vertex, denoted by  $\Gamma^\mu(q, r, -p)$ , as its main ingredient. In Eq. (2.3),  $g$  is the QCD gauge coupling,  $C_f = 4/3$  the Casimir eigenvalue of the fundamental  $SU(3)$  representation, and  $\Delta_{\mu\nu}$  stands for the full gluon propagator in the Landau gauge,

$$\Delta_{\mu\nu}(q) = P_{\mu\nu}(q)\Delta(q), \quad P_{\mu\nu}(q) = g_{\mu\nu} - \frac{q_\mu q_\nu}{q^2}. \quad (2.4)$$

The term  $m$  denotes the current quark mass; throughout this analysis it will be considered to be vanishing,  $m = 0$  (chiral limit). Moreover,

$$\int_q := \int_{\mathbb{R}^4} \frac{d^4 q}{(2\pi)^4}, \quad (2.5)$$

where the use of a symmetry-preserving regularization scheme is implicitly assumed.

After taking appropriate traces, the quark gap equation in Eq. (2.3) is reduced to a set of coupled nonlinear integral equations that determine the dressing functions  $A(p)$  and  $B(p)$ . In particular, we have in Minkowski space

$$\begin{aligned}
B(p) = & -\frac{ig^2C_f}{4} \int_q a(q) \text{Tr} [\gamma^\nu \not{q} \Gamma_2^\mu(q-p, p, -q)] \Delta_{\mu\nu}(q-p) \\
& -\frac{ig^2C_f}{4} \int_q b(q) \text{Tr} [\gamma^\nu \Gamma_1^\mu(q-p, p, -q)] \Delta_{\mu\nu}(q-p), \\
p^2 A(p) = & p^2 + \frac{ig^2C_f}{4} \int_q a(q) \text{Tr} [\not{p} \gamma^\nu \not{q} \Gamma_1^\mu(q-p, p, -q)] \Delta_{\mu\nu}(q-p) \\
& + \frac{ig^2C_f}{4} \int_q b(q) \text{Tr} [\not{p} \gamma^\nu \Gamma_2^\mu(q-p, p, -q)] \Delta_{\mu\nu}(q-p), \tag{2.6a}
\end{aligned}$$

with

$$a(p) := c(p)A(p), \quad b(p) := c(p)B(p), \quad c(p) := \frac{1}{A^2(p)p^2 - B^2(p)}. \tag{2.6b}$$

In Eq. (2.6) we have separated the quark-gluon vertex into the “odd” ( $\Gamma_1$ ) and “even” ( $\Gamma_2$ ) components,

$$\Gamma^\mu(q, r, -p) = \underbrace{\Gamma_1^\mu(q, r, -p)}_{\text{odd \# of } \gamma} + \underbrace{\Gamma_2^\mu(q, r, -p)}_{\text{even \# of } \gamma}. \tag{2.7}$$

(iii) In the Landau gauge, it is natural to consider the “transversely projected” quark-gluon vertex,  $\bar{\Gamma}_\mu(q, r, -p) = P_{\mu\nu}(q) \Gamma^\nu(q, r, -p)$ . In general kinematics,  $\bar{\Gamma}_\mu(q, r, -p)$  can be spanned by eight independent tensors,  $\bar{\tau}_i$ , namely

$$\bar{\Gamma}^\mu(q, r, -p) = \sum_{i=1}^8 \lambda_i(q, r, -p) \bar{\tau}_i^\mu(r, -p), \quad \bar{\tau}_i^\mu(r, -p) = P_\nu^\mu(q) \tau_i^\nu(r, -p), \tag{2.8}$$

where the  $\tau_i^\nu$  in Minkowski space are given by [61, 73–75]

$$\begin{aligned}
\tau_1^\nu(r, -p) &= \gamma^\nu, & \tau_2^\nu(r, -p) &= (p+r)^\nu, \\
\tau_3^\nu(r, -p) &= (\not{p} + \not{r})\gamma^\nu, & \tau_4^\nu(r, -p) &= (\not{p} - \not{r})\gamma^\nu, \\
\tau_5^\nu(r, -p) &= (\not{p} - \not{r})(p+r)^\nu, & \tau_6^\nu(r, -p) &= (\not{p} + \not{r})(p+r)^\nu, \\
\tau_7^\nu(r, -p) &= -\frac{1}{2}[\not{p}, \not{r}]\gamma^\nu, & \tau_8^\nu(r, -p) &= -\frac{1}{2}[\not{p}, \not{r}](p+r)^\nu, \tag{2.9}
\end{aligned}$$

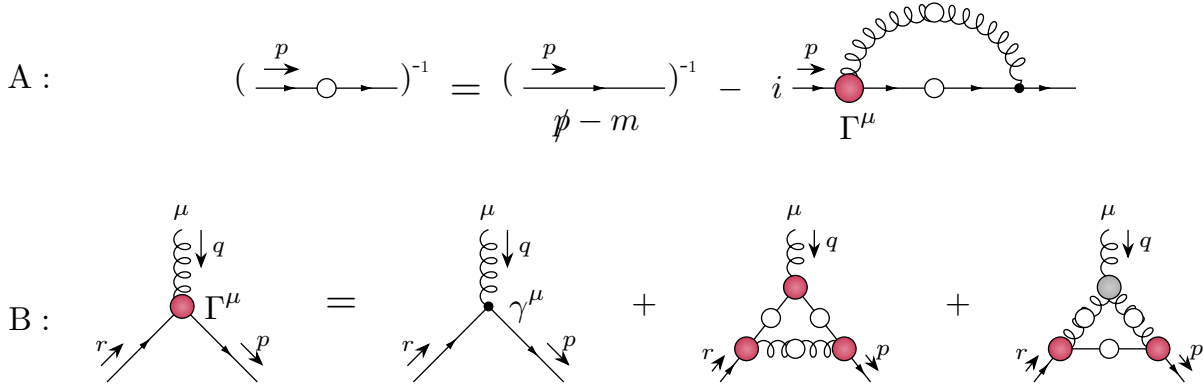


FIG. 1. **Panel A:** Diagrammatic representation of the SDE (gap equation) that determines the quark propagator  $S(p)$ . White circles denote full propagators, red circles stand for full quark-gluon vertices, while small black circles indicate tree-level quark-gluon vertices. **Panel B:** The SDE of the quark-gluon vertex (red circle) obtained within the 3PI formalism. The gray circle denotes the fully-dressed three-gluon vertex.

and the  $\lambda_i(q, r, -p)$  denote form factors that depend on three Lorentz scalars. Within this basis, the component  $\bar{\Gamma}_1^\nu$  is spanned by the elements  $\{\bar{\tau}_1^\nu, \bar{\tau}_5^\nu, \bar{\tau}_6^\nu, \bar{\tau}_7^\nu\}$ , while  $\bar{\Gamma}_2^\nu$  by  $\{\bar{\tau}_2^\nu, \bar{\tau}_3^\nu, \bar{\tau}_4^\nu, \bar{\tau}_8^\nu\}$ .

Within the three-particle-irreducible (3PI) scheme [12, 59, 60], the one-loop dressed SDE that controls the evolution of the form factors  $\lambda_i(q, r, -p)$  is shown diagrammatically in Fig. 1B.

(iii) Instrumental in this entire analysis is the SDE satisfied by the vertex  $\Gamma_5^\mu$ , shown in Fig. 2A. Note that the diagram ( $a_5$ ) contains the fully-dressed quark-gluon vertex  $\Gamma_\nu$ , depicted as the red circle; this graph provides the standard RL description, after the substitution  $\Gamma_\nu \rightarrow \gamma_\nu$ . A key component of this SDE is the “gluon-axial-vector” vertex [1, 7, 35],  $G_5^{ab\mu\nu} = i g t^a \frac{\lambda^b}{2} G_5^{\mu\nu}$ , represented by the yellow circle in diagram ( $b_5$ ) of Fig. 2A. Crucially,  $G_5^{\mu\nu}$  is related to the quark-gluon vertex by the WTI [1, 7]

$$-i P_\mu G_5^{\mu\nu}(P, q, p_2, -q_1) = \Gamma^\nu(q, p_1, -q_1) \gamma_5 + \gamma_5 \Gamma^\nu(q, p_2, -q_2), \quad (2.10)$$

where  $q_i := p_i + q$ . By virtue of Eq. (2.10), when the diagrams contributing to the SDE of  $\Gamma_5^\mu$  are contracted by  $P_\mu$ , the axial WTI of Eq. (2.1) emerges precisely, with the inverse quark propagators satisfying the gap equation with the *full* quark-gluon vertex.

(iv) When the chiral symmetry is dynamically broken, a nonvanishing mass function  $B(p)$  is generated as a solution of Eq. (2.3). As a result, in the limit  $P \rightarrow 0$ ,  $p_1 = p_2 := p$ , the

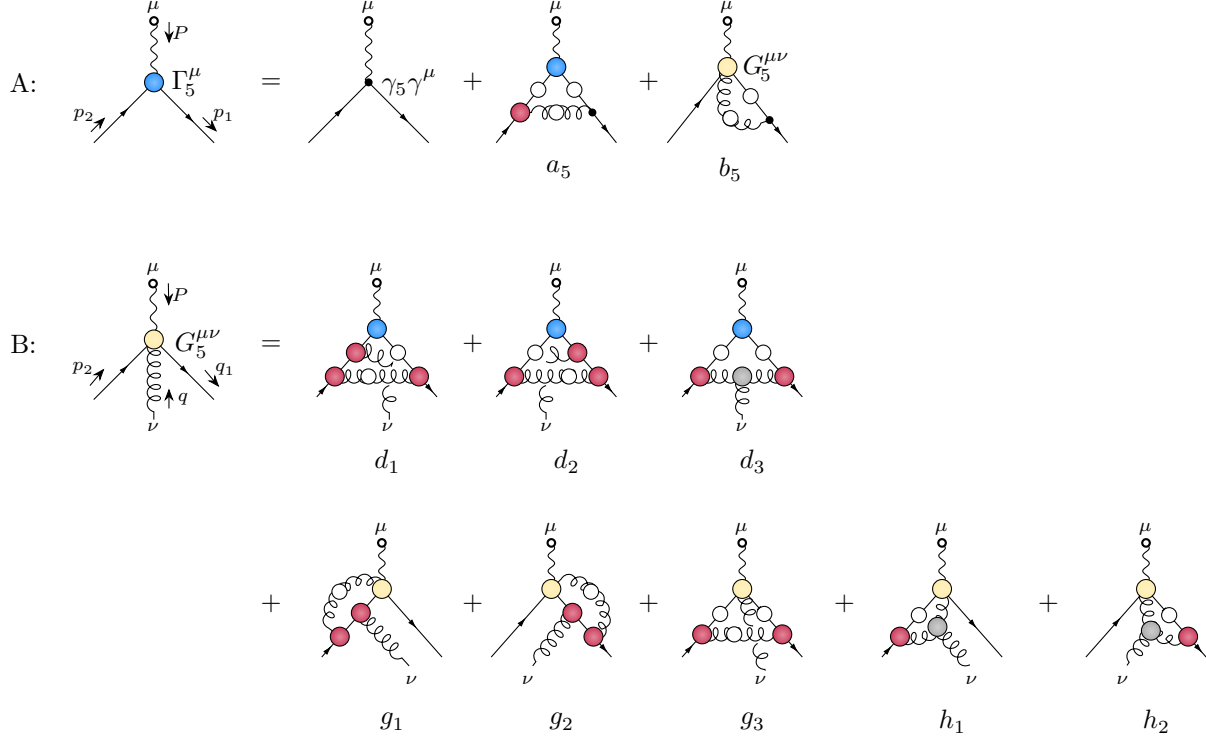


FIG. 2. **Panel A:** The SDE of the axial-vector vertex,  $\Gamma_5^\mu$  (blue circles). The graph ( $b_5$ ) contains the “gluon-axial-vector” vertex,  $G_5^{ab\mu\nu}$  (yellow circle), which is crucial for the preservation of the axial WTI. **Panel B:** The one-loop dressed representation of the gluon-axial-vector vertex; we refer to the graphs  $d_1$ ,  $d_2$ ,  $d_3$  as  $G$ -independent, while to the  $g_1$ ,  $g_2$ ,  $g_3$ ,  $h_1$ ,  $h_2$  as  $G$ -dependent.

WTI of Eq. (2.1) yields

$$\lim_{P \rightarrow 0} P_\mu \Gamma_5^\mu(P, p_2, -p_1) = 2B(p) \gamma_5. \quad (2.11)$$

This result forces  $\Gamma_5^\mu$  to contain a pole term,  $\Gamma_5^\mu(P, p_2, -p_1)|_{\text{pole}}$ , associated with the attendant Nambu-Goldstone boson (pion), of the form

$$\Gamma_5^\mu(P, p_2, -p_1)|_{\text{pole}} = \frac{P^\mu}{P^2} \chi(P, p_2, -p_1) \gamma_5. \quad (2.12)$$

The quantity  $\chi(P, p_2, -p_1)$  is the BSA of the pion, which, in the limit  $P \rightarrow 0$ , is composed by two form factors [70],

$$\chi(0, p, -p) = \chi_1(p) + \chi_3(p) \not{p}. \quad (2.13)$$

The comparison of Eqs. (2.12) and (2.13) furnishes the well-known symmetry-induced relations

$$\chi_1(p) = 2B(p), \quad \chi_3(p) = 0. \quad (2.14)$$

The first relation is particularly powerful, connecting the dominant component of the pion amplitude to the quark mass function.

(v) In the limit  $P \rightarrow 0$ , the SDE that governs the vertex  $\Gamma_5^\mu$  furnishes the BSEs for both  $\chi_1(p)$  and  $\chi_3(p)$ . Quite importantly, as was explicitly shown in [1], these BSEs admit the relations given by Eq. (2.14) as their exact solutions. In that sense, symmetry and dynamics are harmoniously intertwined. Crucial in the demonstration of this key property is the WTI of Eq. (2.10), which, in the limit  $P \rightarrow 0$ , becomes

$$\lim_{P \rightarrow 0} P_\mu G_5^{\mu\nu}(P, q, p_2, -q_1) = 2i\Gamma_2^\nu(q, p, -p - q)\gamma_5. \quad (2.15)$$

(vi) The one-loop dressed approximation of  $G_5^{\mu\nu}$  is given by the diagrams shown in Fig. 2B. It turns out that the contraction of this set of diagrams by  $P_\mu$  generates the r.h.s. of the WTI in Eq. (2.10), where the corresponding quark-gluon vertices  $\Gamma^\nu(q, p_1, -q_1)$  and  $\Gamma^\nu(q, p_2, -q_2)$  satisfy the SDE shown in Fig. 1B [1].

### III. SYMMETRY-PRESERVING TRUNCATION

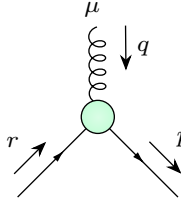
There is a practical difficulty associated with the truncation described in item (vi) of the previous section. Specifically, a subset of the diagrams that define the vertex  $G_5^{\mu\nu}$  in Fig. 2B contain the  $G_5^{\mu\nu}$  itself as their ingredient (second row,  $G$ -dependent graphs), thus converting the dynamical equations for  $\Gamma_5^\mu$  and  $G_5^{\mu\nu}$  into a coupled system. Even though such a system is in principle tractable, it is certainly useful to introduce an operationally simpler approach, which does not compromise the validity of the essential WTIs. In particular, as we demonstrate in this section, one may omit the aforementioned subset of graphs entirely, at the expense of introducing a compensating adjustment at the level of the quark-gluon SDE in Fig. 1B.

The starting point of our truncation is to set  $G_5^{\mu\nu} = 0$  on the r.h.s. of the equation shown in Fig. 2B, thus eliminating the  $G$ -dependent graphs. After doing so, the equation that furnishes  $G_5^{\mu\nu}$  reduces to the three diagrams in the first row of Fig. 2B ( $G$ -independent graphs). However, these remaining diagrams no longer reproduce the WTI of Eq. (2.10), with the full quark-gluon vertices (red circles) satisfying the SDE shown Fig. 1B.

Nonetheless, it turns out that a simplification implemented on the  $\Gamma^\mu$  appearing *inside* all one-loop dressed diagrams in Fig. 1B and Fig. 2B restores the key WTI. Specifically, upon



inspection, one recognizes that the global replacement

$$\Gamma_\mu(q, r, -p) \rightarrow V_\mu(q), \quad V_\mu(q) := \gamma_\mu V(q) = \text{Diagram} \quad , \quad (3.1)$$


gives rise to a symmetry-preserving approximation, defined by the system of equations depicted diagrammatically in the two panels of Fig. 3.

As will become evident from the demonstration leading to Eq. (3.13), the WTI is preserved regardless of the precise form chosen for  $V(q)$ ; the only formal requirement is that  $V(q)$  be function of a single kinematic variable, namely the momentum carried by the gluon. This need arises because, in going from Eq. (3.13) to Eq. (3.7), certain key cancellations take place among various terms upon shifting appropriately the integration variable; these cancellations go through provided that the  $V(q)$  has the aforementioned momentum dependence. The actual expression used for  $V(q)$  in the numerical analysis will be discussed in Sec. VI B.

We emphasize that even though the  $V_\mu(q)$  used as input in the r.h.s. of the SDE in Fig. 3B contains only the classical tensor, the output obtained, represented by the cyan circle, displays the *full* kinematic structure associated with a quark-gluon vertex. In particular, in the Landau gauge, the resulting vertex  $\Gamma^\mu(q, r, -p)$  is composed by eight tensorial structures, see Eq. (2.8), multiplied by the corresponding nonvanishing form factors,  $\lambda_i$ , which depend on three kinematic variables, *e.g.*,  $q^2$ ,  $r^2$  and  $q \cdot r$ . Note that this full vertex will enter in the graph ( $a_5$ ) of the SDE for the axial-vector vertex, thus effectuating the departure from the RL approximation.

Given the above discussion, the closed form of the dynamical equation displayed in Fig. 3B is given by

$$\Gamma^\mu(q, r, -p) = \gamma^\mu + c_1^\mu + c_2^\mu, \quad (3.2)$$

with

$$c_1^\mu = c_a \int_k V^\beta(k) S(p+k) V^\mu(q) S(r+k) V^\alpha(k) \Delta_{\alpha\beta}(k), \quad (3.3)$$

$$c_2^\mu = c_b \int_k V^\beta(k-q) S(r+k) V^\alpha(k) \Delta_{\rho\beta}(k-q) \Delta_{\alpha\delta}(k) \Gamma^{\mu\delta\rho}(q, -k, k-q), \quad (3.4)$$

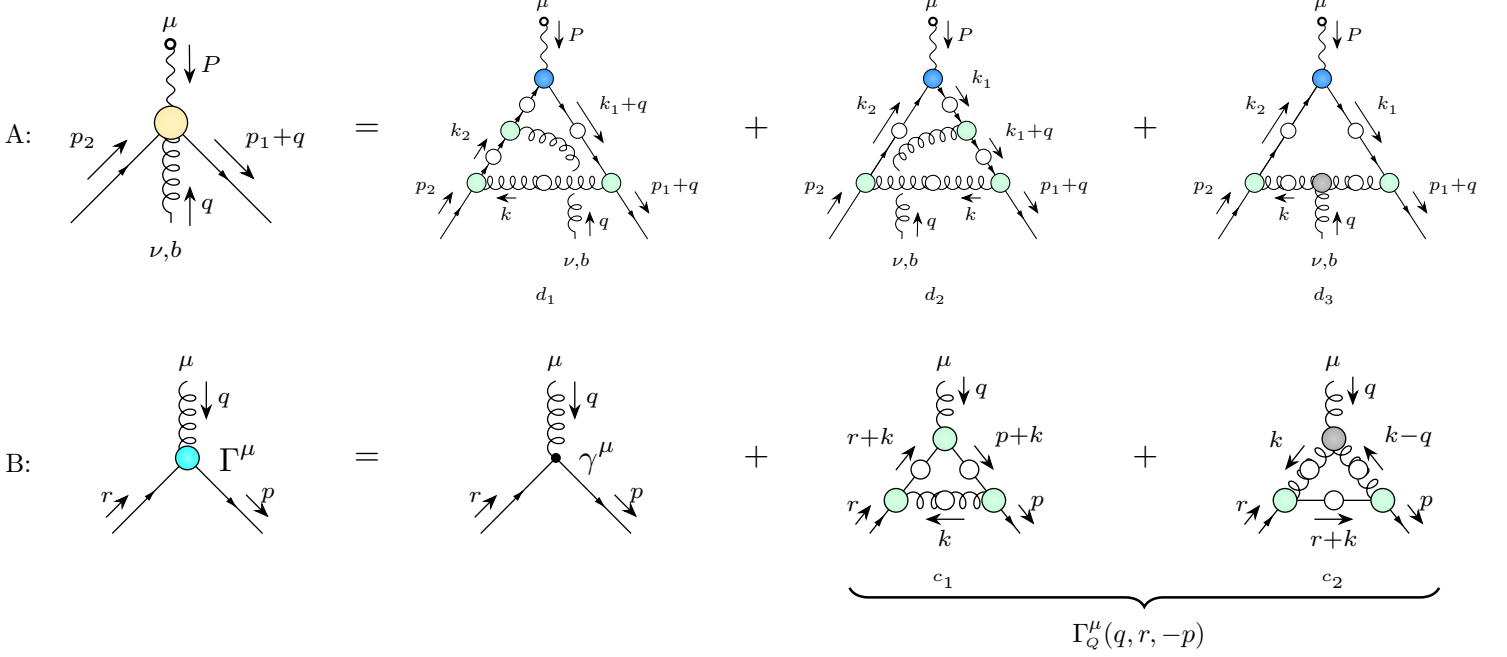


FIG. 3. **Panel A:** The truncated version of the SDE for the vertex  $G_5^{\mu\nu}$ , composed only by  $G$ -independent graphs. The green circles denote the component  $V_\mu$ , defined in Eq. (3.1). **Panel B:** The SDE of the quark-gluon vertex (cyan circle), which is compatible with the truncation of the  $G_5^{\mu\nu}$  shown in the panel above.

where  $\Gamma^{\mu\delta\rho}$  is the full three-gluon vertex,  $c_a = -ig^2(C_f - C_A/2)$ ,  $c_b = -ig^2C_A/2$ , and  $C_A$  is the Casimir eigenvalue of the adjoint representation [ $N$  for  $SU(N)$ ].

It is convenient for what follows to introduce the “quantum” part,  $\Gamma_Q^\mu(q, r, -p)$ , of the quark-gluon vertex, defined and diagrammatically represented as

$$\Gamma_Q^\mu(q, r, -p) = c_1^\mu + c_2^\mu, \quad \Gamma_Q^\mu(q, r, -p) := \text{diagram} \quad (3.5)$$

The diagram shown in the equation is a quark-gluon vertex (cyan circle) with incoming momenta  $r$  and  $p$ , and outgoing momenta  $\mu$  and  $q$ . The vertex is labeled  $\Gamma_Q^\mu$ .

Having set the stage, we next derive the WTI satisfied by the vertex  $G_5^{\mu\nu}$ , given by the diagrams  $d_1$ ,  $d_2$  and  $d_3$  in Fig. 3A,

$$G_5^{\mu\nu}(P, q, p_2, -q_1) = d_1^{\mu\nu} + d_2^{\mu\nu} + d_3^{\mu\nu}. \quad (3.6)$$

Contracting the first two graphs by  $P_\mu$ , and employing Eq. (2.1) under the integral sign, we

get

$$P_\mu d_1^{\mu\nu} = -L_1^\nu - L_3^\nu, \quad P_\mu d_2^{\mu\nu} = -L_2^\nu - L_4^\nu, \quad (3.7)$$

with

$$\begin{aligned} L_1^\nu &= g^2 \kappa_a \int_k V^\beta(k) \gamma_5 S(p_2 + k + q) V^\nu(q) S(p_2 + k) V^\alpha(k) \Delta_{\alpha\beta}(k), \\ L_2^\nu &= g^2 \kappa_a \int_k V^\beta(k) S(p_1 + k + q) V^\nu(q) S(p_1 + k) \gamma_5 V^\alpha(k) \Delta_{\alpha\beta}(k), \\ L_3^\nu &= g^2 \kappa_a \int_k V^\beta(k) S(p_1 + k + q) \gamma_5 V^\nu(q) S(p_2 + k) V^\alpha(k) \Delta_{\alpha\beta}(k), \\ L_4^\nu &= g^2 \kappa_a \int_k V^\beta(k) S(p_1 + k + q) V^\nu(q) \gamma_5 S(p_2 + k) V^\alpha(k) \Delta_{\alpha\beta}(k), \end{aligned} \quad (3.8)$$

where  $\kappa_a = C_f - C_A/2$ . Clearly, since  $V^\nu(q) \gamma_5 + \gamma_5 V^\nu(q) = 0$ , the contributions  $L_3^\nu$  and  $L_4^\nu$  cancel upon addition, giving

$$\begin{aligned} -P_\mu (d_1^{\mu\nu} + d_2^{\mu\nu}) &= g^2 \kappa_a \int_k V^\beta(k) \gamma_5 S(p_2 + k + q) V^\nu(q) S(p_2 + k) V^\alpha(k) \Delta_{\alpha\beta}(k) \\ &\quad + g^2 \kappa_a \int_k V^\beta(k) S(p_1 + k + q) V^\nu(q) S(p_1 + k) \gamma_5 V^\alpha(k) \Delta_{\alpha\beta}(k), \end{aligned} \quad (3.9)$$

or, in terms of the Abelian diagram  $(c_1^\nu)$  shown in [Fig. 3B](#) and given by Eq. (3.3),

$$-iP_\mu (d_1^{\mu\nu} + d_2^{\mu\nu}) = c_1^\nu(q, p_1, -q_1) \gamma_5 + \gamma_5 c_1^\nu(q, p_2, -q_2). \quad (3.10)$$

Similarly, for  $d_3^{\mu\nu}$  we obtain

$$\begin{aligned} -P_\mu d_3^{\mu\nu} &= ig^2 \kappa_b \int_k V^\beta(k') S(p_1 + k) V^\alpha(k) \Gamma^{\nu\rho\delta}(q, -k, k') \Delta_{\alpha\rho}(k) \Delta_{\delta\beta}(k') \gamma_5 \\ &\quad + ig^2 \kappa_b \int_k \gamma_5 V^\beta(k') S(p_2 + k) V^\alpha(k) \Gamma^{\nu\rho\delta}(q, -k, k') \Delta_{\alpha\rho}(k) \Delta_{\delta\beta}(k'), \end{aligned} \quad (3.11)$$

where  $\kappa_b = iC_A/2$  and  $k' = k - q$ . As before, we may express the r.h.s. of Eq. (3.11) in terms of the non-Abelian diagram  $(c_2^\nu)$  in [Fig. 3B](#), given by Eq. (3.4), namely

$$-iP_\mu d_3^{\mu\nu} = c_2^\nu(q, p_1, -q_1) \gamma_5 + \gamma_5 c_2^\nu(q, p_2, -q_2). \quad (3.12)$$

Adding up the results of Eqs. (3.10) and (3.12), and using the definition of  $\Gamma_Q^\mu$  in Eq. (3.5), we find

$$-iP_\mu G_5^{\mu\nu}(P, q, p_2, -q_1) = \Gamma_Q^\mu(q, p_1, -q_1)\gamma_5 + \gamma_5\Gamma_Q^\mu(q, p_2, -q_2). \quad (3.13)$$

Since  $\gamma^\mu\gamma_5 + \gamma_5\gamma^\mu = 0$ , the tree-level terms of the two quark-gluon vertices may be added for free, leading precisely to the WTI of Eq. (2.10), with the quark-gluon vertex defined through the SDE in Eq. (3.2).

Given that the vertex  $G_5^{\mu\nu}$  satisfies Eq. (3.13), the resulting  $\Gamma_5^\mu(P, p_2, -p_1)$  fulfils the axial WTI of Eq. (2.1), where the quark propagator is given by the gap equation in Fig. 1A. Of course, the fully-dressed quark-gluon vertex of the gap equation is now given by Fig. 3B, *i.e.*, the red circle in Fig. 1A must be replaced by the cyan one.

#### IV. PION BSE WITH DRESSED QUARK-GLUON VERTICES

In this section we derive the BSE of the pion by taking the limit  $P \rightarrow 0$  of the SDE for  $\Gamma_5^\mu(P, p_2, -p_1)$ , and then equating the residues of the pole parts appearing on both sides.

The axial-vector vertex  $\Gamma_5^\mu(P, p_2, -p_1)$  arising from the truncation put forth in the previous section may be determined by substituting the  $G_5^{\mu\nu}$  of Fig. 3A into the SDE of Fig. 2A, thus leading to the diagrammatic expansion shown in Fig. 4A. In particular,

$$\Gamma_{5\mu}(P, p_2, -p_1) = \gamma_5\gamma_\mu + a_{5\mu} + b_{5\mu}^1 + b_{5\mu}^2 + b_{5\mu}^3, \quad (4.1)$$

with

$$\begin{aligned} a_{5\mu} &= c_d \int_q \gamma^\sigma S(q_1) \Gamma_{5\mu}(P, q_2, -q_1) \Gamma^\nu(q, p_2, -q_2) \Delta_{\nu\sigma}(q), \\ b_{5\mu}^i &= -ic_d \int_q \gamma^\sigma S(q_1) d_{i\mu}^{\nu\sigma}(P, q, p_2, -q_2) \Delta_{\nu\sigma}(q), \quad i = 1, 2, 3, \end{aligned} \quad (4.2)$$

where we defined  $c_d = -ig^2 C_f$  and  $q_i = p_i + q$ . The terms  $d_i^{\mu\nu}$  are those composing the vertex  $G_5^{\mu\nu}$ , shown in Fig. 3A.

After contracting the SDE in Eq. (4.1) by  $P_\mu$ , taking the limit  $P \rightarrow 0$  to isolate its pole contribution, and finally eliminating  $\gamma_5$  from both sides of the resulting equation, the pion BSE shown in Fig. 4B emerges. Specifically, using that  $S(p)S(-p) = -c(p)$ , with  $c(p)$  defined in Eq. (2.6b), the BSE assumes the form

$$\chi(p) = a_\chi + b_\chi^1 + b_\chi^2 + b_\chi^3, \quad (4.3)$$

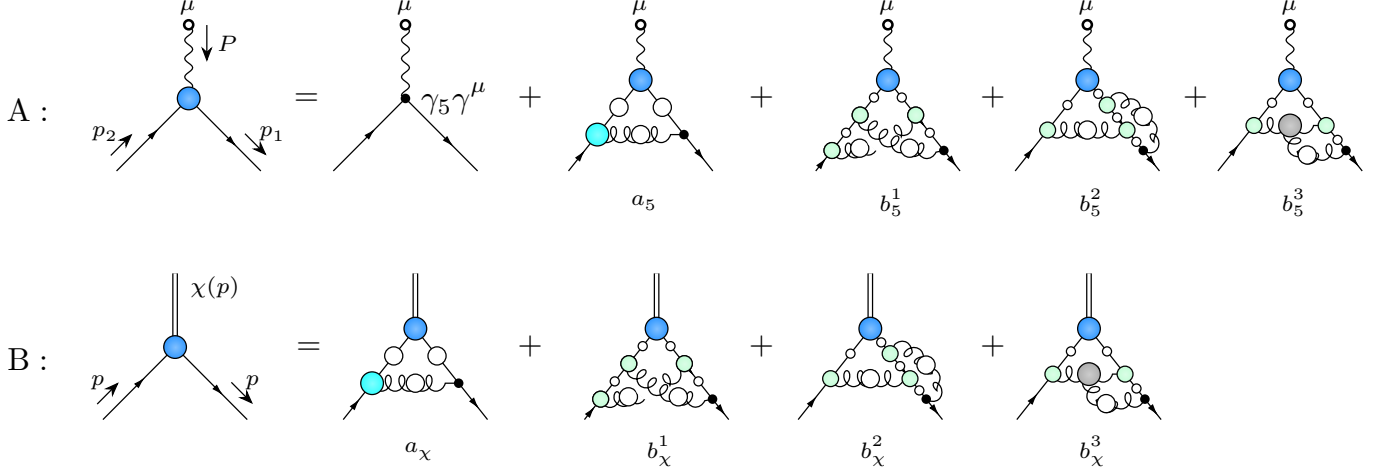


FIG. 4. **Panel A:** The SDE for the axial-vector vertex, emerging once the truncation for the  $G_5^{\mu\nu}$  shown in Panel A of Fig. 3 has been implemented. **Panel B:** The pion BSE, obtained after contracting the SDE in the panel above with  $P_\mu$  and then taking the limit  $P \rightarrow 0$ .

with

$$\begin{aligned}
 a_\chi &= -c_d \int_q \gamma^\sigma c(q') \chi(p) [\Gamma_2^\nu(q, p, -q') - \Gamma_1^\nu(q, p, -q')] \Delta_{\nu\sigma}(q), \\
 b_\chi^1 &= -c_d c_a \int_{q,k} \gamma^\sigma S(q') V^\beta(k) c(q' + k) \chi(q' + k) V^\nu(q) S(-k - p) V^\alpha(k) \Delta_{\alpha\beta}(k) \Delta_{\nu\sigma}(q), \\
 b_\chi^2 &= c_d c_a \int_{q,k} \gamma^\sigma S(q') V^\beta(k) S(q' + k) V^\nu(q) c(p + k) \chi(p + k) V^\alpha(k) \Delta_{\alpha\beta}(k) \Delta_{\nu\sigma}(q), \\
 b_\chi^3 &= c_d c_b \int_{q,k} \gamma^\sigma S(q') V^\beta(k') c(p + k) \chi(p + k) V^\alpha(k) \Gamma^{\nu\rho\delta}(q, -k, k') \Delta_{\alpha\rho}(k) \Delta_{\delta\beta}(k') \Delta_{\nu\sigma}(q),
 \end{aligned} \tag{4.4}$$

where  $q' = p + q$ ,  $k' = k - q$ .

Clearly, the terms  $a_\chi$  and  $b_\chi^{(i)}$  in the BSE of Eq. (4.3) are in one-to-one correspondence with the diagrams  $a_5$  and  $b_5^i$  of the axial-vector vertex SDE in Eq. (4.1).

In particular, we can now project out the dynamical equation for  $\chi_1$ , by simply taking the trace in Eq. (4.3), namely

$$\chi_1(p) = \frac{1}{4} \text{Tr} [a_\chi + b_\chi^1 + b_\chi^2 + b_\chi^3]. \tag{4.5}$$

The traces on the r.h.s. of Eq. (4.5) can be evaluated using the expressions collected in

Eq. (4.4), yielding

$$\begin{aligned}
\text{Tr}(a_\chi) &= c_d \int_q c(q') \chi_1(q') \text{Tr} [\gamma^\sigma \Gamma_1^\nu(q, p, -q')] \Delta_{\nu\sigma}(q), \\
\text{Tr}(b_\chi^1) &= -c_d c_a \int_{q,k} c(t_2) \chi_1(t_2) \text{Tr} [\gamma^\sigma S(q') \gamma^\beta \gamma^\nu S(-t_1) \gamma^\alpha] V^2(k) V(q) \Delta_{\alpha\beta}(k) \Delta_{\nu\sigma}(q), \\
\text{Tr}(b_\chi^2) &= c_d c_a \int_{q,k} c(t_1) \chi_1(t_1) \text{Tr} [\gamma^\sigma S(q') \gamma^\beta S(t_2) \gamma^\nu \gamma^\alpha] V^2(k) V(q) \Delta_{\alpha\beta}(k) \Delta_{\nu\sigma}(q), \\
\text{Tr}(b_\chi^3) &= c_d c_b \int_{q,k} c(t_1) \chi_1(t_1) \text{Tr} [\gamma^\sigma S(q') \gamma^\beta \gamma^\alpha] V^2(k) \Gamma^{\nu\rho\delta}(q, -k, k') \Delta_{\alpha\rho}(k) \Delta_{\delta\beta}(k') \Delta_{\nu\sigma}(q),
\end{aligned} \tag{4.6}$$

where  $t_1 = p + k$  and  $t_2 = t_1 + q$ .

We note that the cyan vertex enters into the standard diagram  $a_5$ , thus effectuating the transition beyond the RL approximation. In that sense, the remaining three diagrams,  $b_5^{(1)}$ ,  $b_5^{(2)}$ , and  $b_5^{(3)}$  are required precisely for restoring the symmetry.

## V. RENORMALIZATION OF THE SDE-BSE SYSTEM

The final system that one must solve consists of three dynamical equations, namely (a) the SDE of the quark propagator (gap equation) given in Eq. (2.3), with  $m = 0$ , (b) the SDE of the quark-gluon vertex in Eq. (3.2), and (c) the pion BSE in Eq. (4.5).

Before proceeding with the numerical treatment, this set of equations must be properly renormalized. The renormalization proceeds in the standard way, by means of the following relations

$$\begin{aligned}
\Delta_R(q) &= Z_3^{-1} \Delta(q), & S_R(q) &= Z_2^{-1} S(q), \\
\Gamma_R^\mu(r, p, q) &= Z_1 \Gamma^\mu(r, p, q), & \chi_1^R(q) &= Z_4 \chi_1(q), \\
g_R &= Z_1^{-1} Z_2 Z_3^{1/2} g,
\end{aligned} \tag{5.1}$$

which connect bare and unrenormalized quantities by means of the corresponding (cutoff-dependent) renormalization constants  $Z_i$ , with  $i = 1, 2, 3, 4$ . Note that the requirement that the fundamental WTI of Eq. (2.1) should maintain its form intact after renormalization,

imposes the constraint  $Z_4 = Z_2$ . In any case, due to the linearity and homogeneity of the BSE in Eq. (4.5), see Fig. 4B, the constant  $Z_4$  drops out automatically from both sides.

For the renormalization scheme, we adopt a variant of momentum subtraction (MOM) [76], denoted  $\widetilde{\text{MOM}}$  [60, 77–79]. This scheme is defined by prescribing that at the renormalization point  $\mu$ , the propagators reduce to their tree-level forms,

$$\Delta(\mu) = \mu^{-2}, \quad A(\mu) = 1, \quad (5.2)$$

and that the classical form factor,  $\lambda_1(q, r, -p)$ , attains its tree-level value in the soft-gluon limit, *i.e.*,

$$\lambda_1(0, p, -p)|_{p^2=\mu^2} = 1. \quad (5.3)$$

We emphasize that although this is an exceptional kinematic configuration,  $\lambda_1(0, p, -p)$  is infrared finite [80], thus defining a valid scheme for the subtraction of ultraviolet divergences.

Employing the above relations, it is straightforward to show that the renormalized gap equation is given by

$$S_{\text{R}}^{-1}(p) = Z_2 \not{p} + i g_{\text{R}}^2 C_f Z_1 \int_q \gamma^\nu S_{\text{R}}(q) \Gamma_{\text{R}}^\mu(q - p, p, -q) \Delta_{\mu\nu}^{\text{R}}(q - p). \quad (5.4)$$

Similarly, the renormalized SDE of the quark-gluon vertex reads

$$\Gamma_{\text{R}}^\mu(q, r, -p) = Z_1 \gamma^\mu + c_{1\text{R}}^\mu + c_{2\text{R}}^\mu, \quad (5.5)$$

where the index “R” on  $c_{1,2}$  indicates that all quantities appearing in the expressions given in Eqs. (3.3) and (3.4) have been replaced by their renormalized counterparts. Finally, the renormalized BSE has the form

$$\chi_1^{\text{R}}(p) = \frac{1}{4} Z_1 \text{Tr} [a_\chi^{\text{R}} + b_\chi^{1,\text{R}} + b_\chi^{2,\text{R}} + b_\chi^{3,\text{R}}], \quad (5.6)$$

where, again, the index “R” on the r.h.s. denotes that renormalized ingredients have been inserted in the relations of Eq. (4.4). In what follows we suppress the index “R”, in order to simplify the notation.

We note that, in both Eqs. (5.4) and (5.6), the  $Z_1$  appears multiplicatively, essentially due to the fact that there is a tree-level quark-gluon vertex in each of the diagrams defining these contributions. The presence of  $Z_1$  is crucial for the cancellation of overlapping divergences [81–86].

In what follows we will implement the multiplicative renormalizability by relying on an expedient often utilized in the literature, mainly in the context of the quark gap equation [67–69]. In particular, denoting the kernel of the gap equation by  $\mathcal{K}_{\text{gap}}(p, q, t)$ , with  $t = q - p$ , one carries out the *effective* replacement

$$Z_1 \mathcal{K}_{\text{gap}}(p, q, t) \rightarrow \mathcal{C}(t) \mathcal{K}_{\text{gap}}(p, q, t), \quad (5.7)$$

where, for large momenta, the function  $\mathcal{C}(t)$ , evolves as the classical form factor of the quark-gluon vertex [*i.e.*, the anomalous dimension of  $\lambda_1$  in the symmetric limit ( $q^2 = r^2 = p^2$ )].

Adopting this procedure, the gap equation reads

$$Z_1 \int_q \gamma^\nu S(q) \Gamma^\mu(q-p, p, -q) \Delta_{\mu\nu}^{\text{R}}(q-p) \rightarrow \int_q \gamma^\nu \mathcal{C}(q-p) S(q) \Gamma^\mu(q-p, p, -q) \Delta_{\mu\nu}^{\text{R}}(q-p). \quad (5.8)$$

Importantly, Eqs. (3.1) and (5.9) imply that  $V(t)$  and  $\mathcal{C}(t)$  scale as the quark-gluon vertex under a change of the renormalization point. Therefore, the combination  $g^2 \mathcal{C} \Sigma \Gamma \Delta$  is guaranteed to be renormalization-group-invariant.

It is clear that if the substitution in Eq. (5.7) is carried out at the level of the gap equation, the preservation of the WTI in Eq. (2.1) requires a similar replacement at the level of the SDE for  $\Gamma_5^\mu(P, p_2, -p_1)$ , see Fig. 4A, and, finally, of the pion BSE derived from it. In particular, a factor  $\mathcal{C}(t)$  is introduced in all terms of Eq. (4.6), and the  $Z_1$  is removed from Eq. (5.6). Note that the argument of  $\mathcal{C}(t)$  coincides with the momentum of the gluon that enters in the tree-level vertex of each diagram.

While the asymptotic form of  $\mathcal{C}(t)$  is fixed by resorting to renormalization-group arguments, its infrared completion remains undetermined. In the related studies [67–69], appropriate *Ansätze* have been used for the infrared part of  $\mathcal{C}(t)$ , which have the additional effect of increasing the required strength of the gap equation kernel. Given that a function with these characteristics, namely the  $V(q)$  in Eq. (3.1), has already been introduced, in what follows we opt for the natural choice

$$\mathcal{C}(t) \rightarrow V(t), \quad (5.9)$$

thus obtaining for the quark gap equation

$$S^{-1}(p) = Z_2 \not{p} + i g^2 C_f \int_q \gamma^\nu V(q-p) S(q) \Gamma^\mu(q-p, p, -q) \Delta_{\mu\nu}(q-p). \quad (5.10)$$



Similarly, the pion BSE becomes

$$\chi_1(p) = \frac{1}{4} \text{Tr} \left[ \tilde{a}_\chi + \tilde{b}_\chi^1 + \tilde{b}_\chi^2 + \tilde{b}_\chi^3 \right], \quad (5.11)$$

with

$$\begin{aligned} \text{Tr}(\tilde{a}_\chi) &= c_d \int_q c(q') \chi_1(q') \text{Tr} \left[ \gamma^\sigma \Gamma_1^\nu(q, p, -q') \right] V(q) \Delta_{\nu\sigma}(q), \\ \text{Tr}(\tilde{b}_\chi^1) &= -c_d c_a \int_{q,k} c(t_2) \chi_1(t_2) \text{Tr} \left[ \gamma^\sigma S(q') \gamma^\beta \gamma^\nu S(-t_1) \gamma^\alpha \right] V^2(k) V^2(q) \Delta_{\alpha\beta}(k) \Delta_{\nu\sigma}(q), \\ \text{Tr}(\tilde{b}_\chi^2) &= c_d c_a \int_{q,k} c(t_1) \chi_1(t_1) \text{Tr} \left[ \gamma^\sigma S(q') \gamma^\beta S(t_2) \gamma^\nu \gamma^\alpha \right] V^2(k) V^2(q) \Delta_{\alpha\beta}(k) \Delta_{\nu\sigma}(q), \\ \text{Tr}(\tilde{b}_\chi^3) &= c_d c_b \int_{q,k} c(t_1) \chi_1(t_1) \text{Tr} \left[ \gamma^\sigma S(q') \gamma^\beta \gamma^\alpha \right] V^2(k) V(q) \Gamma^{\nu\rho\delta}(q, -k, k') \Delta_{\alpha\rho}(k) \Delta_{\delta\beta}(k') \Delta_{\nu\sigma}(q). \end{aligned} \quad (5.12)$$

It turns out that the multiplication of the terms given in Eq. (5.12) by  $V(t)$  leads to a considerable simplification in the form of the BSE. In particular, as one may appreciate in Fig. 5A, the sum of  $\tilde{b}_\chi^2$  and  $\tilde{b}_\chi^3$  generates precisely the quantum part  $\Gamma_Q^\mu$  of the quark-gluon vertex, as defined in Eq. (3.5) and in Fig. 3B. Therefore, the BSE assumes the final form shown in Fig. 5B, namely

$$4\chi_1(p) = (a) + (b) + (c), \quad (5.13)$$

with

$$\begin{aligned} \text{dressed RL: } (a) &= c_d \int_q c(q') \chi_1(q') \text{Tr} \left[ \gamma^\sigma \Gamma_1^\nu(q, p, -q') \right] V(q) \Delta_{\nu\sigma}(q), \\ \text{quantum: } (b) &= c_d \int_q c(q') \chi_1(q') \text{Tr} \left[ \Gamma_{Q,1}^\sigma(-q, q', -p) \gamma^\nu \right] V(q) \Delta_{\nu\sigma}(q), \\ \text{crossed: } (c) &= -c_d c_a \int_{q,k} c(t_2) \chi_1(t_2) \text{Tr} \left[ \gamma^\sigma S(q') \gamma^\beta \gamma^\nu S(-t_1) \gamma^\alpha \right] V^2(k) V^2(q) \Delta_{\alpha\beta}(k) \Delta_{\nu\sigma}(q), \end{aligned} \quad (5.14)$$

where  $\Gamma_{Q,1}^\sigma$  denotes the quantum part of the vertex with an odd number of Dirac  $\gamma$  matrices. We note that the tensorial structures associated with the form factors  $\lambda_5$  and  $\lambda_7$  drop out from the above equations for the same reason described in Sec. VI C, in connection with the equation for  $B(p)$ ; thus the only active components are  $\lambda_1$  and  $\lambda_6$ .

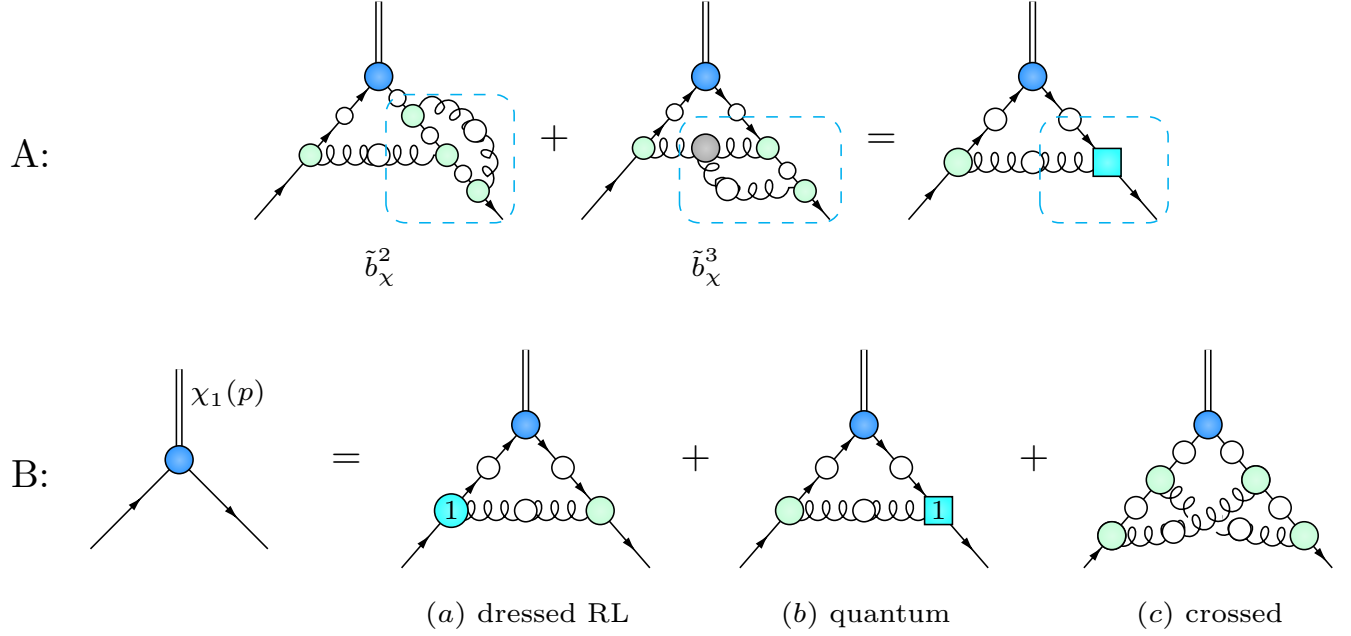


FIG. 5. **Panel A:** The diagrammatic formation of  $\Gamma_Q$ , once the effective renormalization has been carried out. **Panel B:** The final form of the BSE after renormalization. Diagram (a) is denominated “dressed RL” because it corresponds to the standard RL diagram, but now dressed with a full quark-gluon vertex, diagram (b) is called “quantum” because it contains the quantum part of the same vertex, while diagram (c), which is named “crossed” due to its geometry, contains only the  $V$ .

## VI. NUMERICAL ANALYSIS

In this section we carry out the numerical analysis required for the solution of the system of dynamical equations, consisting of the quark-gap equation, the SDE of the quark-gluon vertex, and the BSE of the pion.

### A. Inputs

We begin with a presentation of the inputs used in this work, namely the gluon propagator, the leading form factor of the three-gluon vertex, the value of the strong coupling, and the form of the function  $V(q)$ .

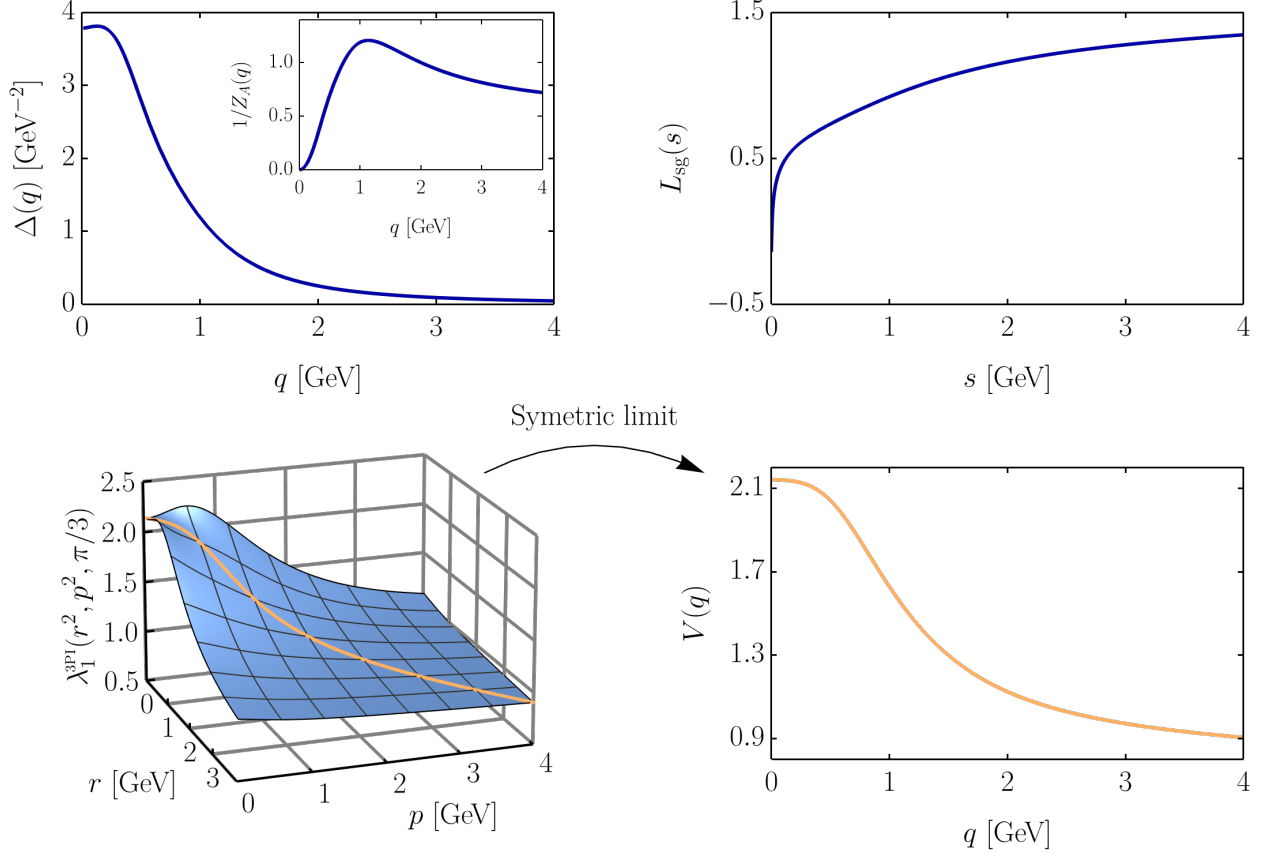


FIG. 6. The input functions employed in the numerical solution of the SDE-BSE system. **Upper left:** The gluon propagator, corresponding to the lattice data of [87, 88], and the corresponding dressing function (inset); **Upper right:** The form factor  $L_{sg}(s)$  of the three-gluon vertex, given in Eq. (A1) of [79]; **Lower left:** The classical form factor of the quark-gluon vertex obtained in [60], for  $\theta_{rp} = \pi/3$ ; the orange line indicates the diagonal  $r^2 = p^2$ , corresponding to the symmetric configuration, and **Lower right:** The function  $V(q)$ , identified with the diagonal of the previous panel, plotted in isolation.

### 1. Gluon propagator

All integral equations entering in our analysis share as common ingredient the Landau-gauge gluon propagator  $\Delta_{\mu\nu}(q)$ , defined in Eq. (2.4). For its scalar part,  $\Delta(q)$ , we use a fit to the lattice data of [87, 88], where the gluon propagator was simulated with two active quark flavours,  $N_f = 2$ . The  $\Delta(q)$  employed is displayed in the upper left panel of Fig. 6, renormalized at  $\mu = 2$  GeV. The functional form of the fit is described in Eq. (A1) of [79], and has been employed in the computation of the quark-gluon vertex presented in [60].

Note that the dynamical quarks entering in this propagator possess non-vanishing current masses, since the chiral limit may not be simulated on the lattice. Even though our analysis is carried out in the chiral limit, this discrepancy has no practical consequences. This may be clearly seen from the work of [74], where the gluon dressing function,  $1/Z_A(q) = q^2 \Delta(q)$  with  $N_f = 2$  quark flavours was obtained for a variety of pion masses. As is evident from Fig. 4a therein, the  $1/Z_A(q)$  is essentially insensitive to the value of the pion masses, within the range  $m_\pi \in [285, 60]$  MeV. This lack of sensitivity persists until the chiral limit,  $m_\pi = 0$ , as one may deduce from the right panel of Fig. 2 in [89]. Specifically, the lowest pion mass reached in [74], namely  $m_\pi = 60$  MeV, corresponds to a current quark mass of approximately  $m \approx 1$  MeV. Between this value and the chiral limit,  $m = 0$ , the pion mass drops rather abruptly from  $m_\pi = 60$  MeV down to  $m_\pi = 0$ . However, varying  $m$  within the narrow interval  $[0, 1]$  MeV at the level of the quark gap equation leaves the functions  $A(p)$  and  $M(p)$  practically unchanged. Given that the dependence of the gluon propagator on the quark parameters is fairly mild, of the type  $\ln[p^2 + M^2(p)]$ , see e.g., [61], no appreciable effects are induced into the  $1/Z_A(q)$  until the chiral limit has been reached.

## 2. Three-gluon vertex

The three-gluon vertex,  $\Gamma_{\alpha\beta\gamma}(q, r, p)$ , enters in the non-Abelian graph,  $c_2$ , of the quark-gluon vertex SDE, shown in Fig. 3B, as well as in the BSE of Eq. (5.13), through the “quantum” diagram shown in Fig. 5A. Since, in the Landau gauge, the three-gluon vertex is contracted by the three projection operators associated with each one of its legs, it is natural to introduce the transversely-projected vertex  $\bar{\Gamma}^{\mu\nu\rho}(q, r, p) = P_\alpha^\mu(q)P_\beta^\nu(r)P_\gamma^\rho(p)\Gamma^{\alpha\beta\gamma}(q, r, p)$ . As was shown in a series of works [34, 90–94], one may capitalize on the key property of “planar-degeneracy”, and achieve a very accurate description of  $\bar{\Gamma}^{\mu\nu\rho}(q, r, p)$  by retaining only its tree-level structure  $\bar{\Gamma}_0^{\mu\nu\rho}(q, r, p)$ , namely

$$\bar{\Gamma}^{\mu\nu\rho}(q, r, p) = L_{sg}(s)\bar{\Gamma}_0^{\mu\nu\rho}(q, r, p), \quad s^2 = \frac{1}{2}(q^2 + r^2 + p^2), \quad (6.1)$$

where

$$\Gamma_0^{\mu\nu\rho}(q, r, p) = g^{\nu\rho}(r - p)^\mu + g^{\mu\rho}(p - q)^\nu + g^{\mu\nu}(q - r)^\rho. \quad (6.2)$$

A fit for the form factor  $L_{sg}(s)$  is given in Eq. (A1) of [79]; the resulting curve is shown in the upper right panel of Fig. 6. Note that in the  $\widetilde{\text{MOM}}$  scheme, defined by Eqs. (5.2)

$d$	$\kappa^2$	$b_0^2$	$b_1^2$ [GeV <sup>2</sup> ]	$b_2^2$ [GeV <sup>2</sup> ]	$b_3^2$ [GeV <sup>2</sup> ]	$e_0^2$ [GeV <sup>2</sup> ]	$e_1^2$ [GeV <sup>2</sup> ]
1.154	1.774	0.0145	126.113	217.268	4.766	3.916	2.079

TABLE I. Best fit parameters for  $V(q)$  to reproduce the symmetric slice ( $q^2 = r^2 = p^2$ ) of  $\lambda_1^{3\text{PI}}$  as obtained in [60].

and (5.3),  $L_{sg}(\mu) \neq 1$ . The conversion between the  $\widetilde{\text{MOM}}$  scheme and the asymmetric MOM scheme [92, 95], wherein  $L_{sg}^{asym}(\mu) = 1$ , amounts to a finite rescaling  $L_{sg}(s) = 1.16 L_{sg}^{asym}(s)$  for  $\mu = 2$  GeV (see App. B of [79]).

### 3. Strong coupling

For the value of the coupling in the  $\widetilde{\text{MOM}}$  scheme, we adopt the estimate  $\alpha_s(\mu) = 0.55$  at  $\mu = 2$  GeV. This value was estimated in [60] by adjusting the solution of the one-loop dressed SDE for the quark-gluon vertex to the lattice data of [78] for the soft-gluon  $\lambda_1(0, p, -p)$ , computed with  $N_f = 2$  dynamical quarks.

### 4. The function $V(q)$

The last ingredient needed for our study is an expression for  $V(q)$ . In order to maintain a close connection to the full quark-gluon vertex, we identify  $V(q)$  with the symmetric limit of the classical form factor obtained in the analysis of [60].

In that study, the SDE shown in Fig. 1B was solved iteratively, having full quark-gluon vertices inside the defining integrals instead of a  $V(q)$ . In Euclidean space, we will express all form factors as functions of  $r^2$ ,  $p^2$  and  $\theta_{rp}$ ,

$$\lambda_i(q, r, -p) \rightarrow \lambda_i(r^2, p^2, \theta_{rp}). \quad (6.3)$$

In particular the form factor associated with  $\bar{\tau}_1^\mu = P_\nu^\mu(q)\gamma^\nu$  is denoted by  $\lambda_i^{3\text{PI}}(r^2, p^2, \theta_{rp})$ . The solution for the special value  $\theta_{rp} = \pi/3$  is shown in the lower left panel of Fig. 6. The orange curve marked on that plot is the diagonal,  $p^2 = r^2$ , which coincides with the so-called “symmetric limit”. When expressed in terms of the three momenta, this limit corresponds to  $q^2 = r^2 = p^2$ , in which case, given that  $q = p - r$ , one finds indeed that  $\theta_{rp} = \pi/3$ .

In what follows we identify  $V(q)$  with the orange curve corresponding to the symmetric limit in Fig. 6, namely  $(r^2, p^2 \rightarrow q^2)$

$$V(q) := \lambda_1^{3\text{PI}}(q^2, q^2, \pi/3). \quad (6.4)$$

For this particular curve we employ the fit

$$V(q) = \frac{d}{U(q)^{\frac{9}{4\beta_0}} + R(q)}, \quad (6.5)$$

where  $\beta_0 = 11 - 2N_f/3$ , and

$$U(q) = 1 + \kappa \log \left( \frac{q^2 + \eta(q)}{\mu^2 + \eta(q)} \right), \quad R(q) = \frac{b_0^2 + \frac{q^2}{b_1^2}}{1 + \frac{q^2}{b_2^2} + \left( \frac{q^2}{b_3^2} \right)^2}, \quad \eta(q) = \frac{e_0^2}{1 + \frac{q^2}{e_1^2}}, \quad (6.6)$$

are functions adjusted to reproduce the  $\lambda_1^{3\text{PI}}(q^2, q^2, \pi/3)$  from [60], at the renormalization scale of  $\mu = 2$  GeV. The optimal values for the fit parameters are collected in Tab. I, and the resulting curve for  $V(q)$  is displayed in the lower right panel of Fig. 6. Note that in the  $\widetilde{\text{MOM}}$  renormalization scheme,  $V(\mu) = 1.12$ .

## B. Quark-gluon vertex

In order to treat the SDE of Eq. (3.2) numerically, one must first implement the transition to Euclidean space; we do so by following the conversion rules exposed in detail in [60], see in particular Section IV. B and Appendix A therein.

Substituting into the Euclidean SDE the relevant ingredients discussed in Sec. VI A, one may obtain the form factors  $\lambda_i$  through simple integration.

The corresponding results for the chirally symmetric form factors  $\lambda_{1,5,6,7}$ , which compose the  $\bar{\Gamma}_1^\nu$ , are shown in Fig. 7. The chiral symmetry breaking form factors  $\lambda_{2,3,4,8}$ , which compose  $\bar{\Gamma}_2^\nu$ , are displayed in Fig. 8.

In the upper left panel of Fig. 7 we present a direct comparison between the  $\lambda_1$  acquired using the  $V(q)$  as input and the  $\lambda_1^{3\text{PI}}$  obtained from the full treatment of [60]; the latter quantity is also shown in the lower left panel of Fig. 6, where its diagonal is identified with the  $V(q)$ . We note that the two form factors compare rather well through the entire kinematic range, showing relatively mild deviations in the infrared region.

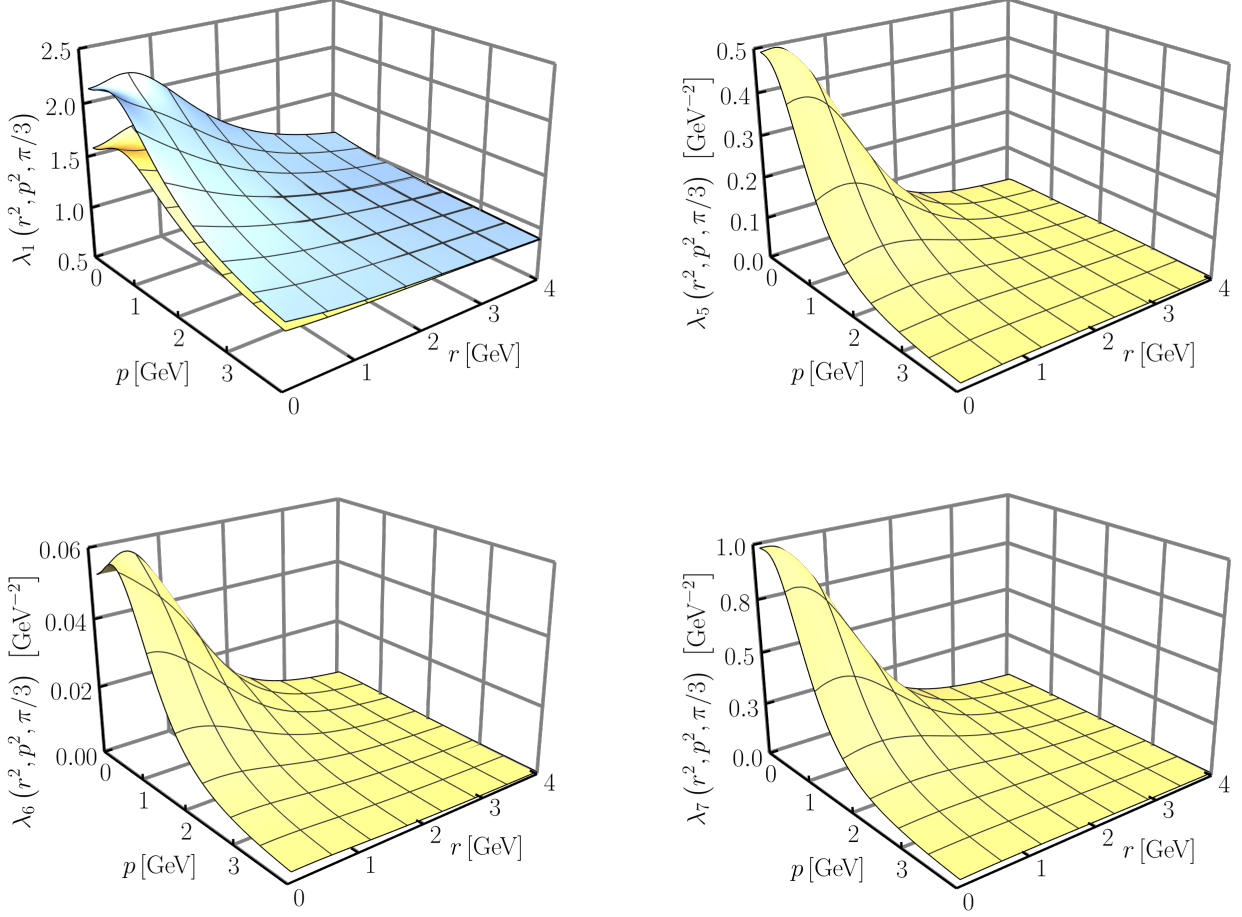


FIG. 7. The chirally symmetric form factors  $\lambda_i$ ,  $i = 1, 5, 6, 7$ , of the quark-gluon vertex, plotted as functions of the momenta  $r$  and  $p$ , for a fixed value of the angle  $\theta_{rp}$  formed between them,  $\theta_{rp} = \pi/3$ . In the upper left panel we include a comparison with the form factor  $\lambda_1^{3\text{PI}}$  (blue surface), also shown in the lower left panel of Fig. 6.

### C. Gap equation

After passing to Euclidean space following standard conventions, the discretization of the momentum dependence using Gaussian quadratures transforms the integral equations into a system of non-linear algebraic equations. These equations are solved by fixed-point iteration: starting from an initial guess for  $A(p)$  and  $B(p)$ , the loop integrals are evaluated numerically, and the dressing functions are updated until convergence is achieved [96]. The corresponding results are shown in Fig. 9. In the left panel, we show the result for the function  $B(p)$ , while the function  $A(p)$  is displayed in the inset.

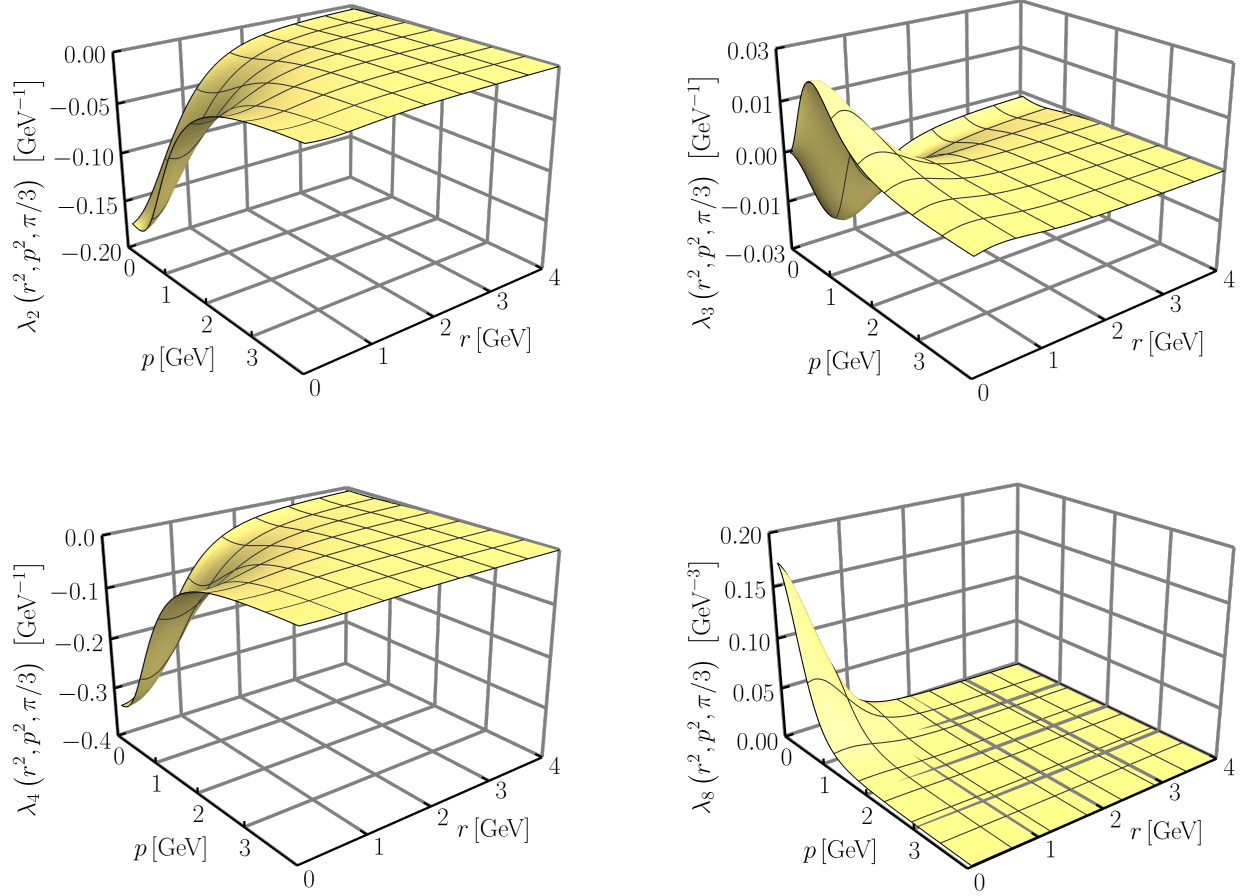


FIG. 8. The chiral symmetry breaking quark-gluon vertex form factors  $\lambda_i$ ,  $i = 2, 3$  (upper panel) and  $i = 4, 8$  (lower panel) plotted as functions of the quark-momenta  $r$  and  $p$  for a fixed value  $\theta_{rp} = \pi/3$ .

The numerical solution for the corresponding constituent quark mass,  $\mathcal{M}(p) = B(p)/A(p)$ , is displayed in the right panel of Fig. 9 as a continuous blue curve. In that figure, we also show, as a dashed orange curve, the mass obtained if we solve the gap equation with a quark-gluon vertex that contains only the classical component, *i.e.*,  $\bar{\Gamma}^\mu \rightarrow \lambda_1 \bar{\tau}_1^\mu$ . As we see, the two results are relatively close, which indicates that the bulk of the mass originates from the classical tensor structure. The rôle of the remaining form factors is to enhance the mass by about 7% at the origin and 30% at  $p = 1$  GeV. We find that the second most important component is the one associated with the form factor  $\lambda_4$ , in agreement with earlier observations presented in [61].

Lastly, we point out that the form factors  $\lambda_5$  and  $\lambda_7$  do not contribute to the equation for



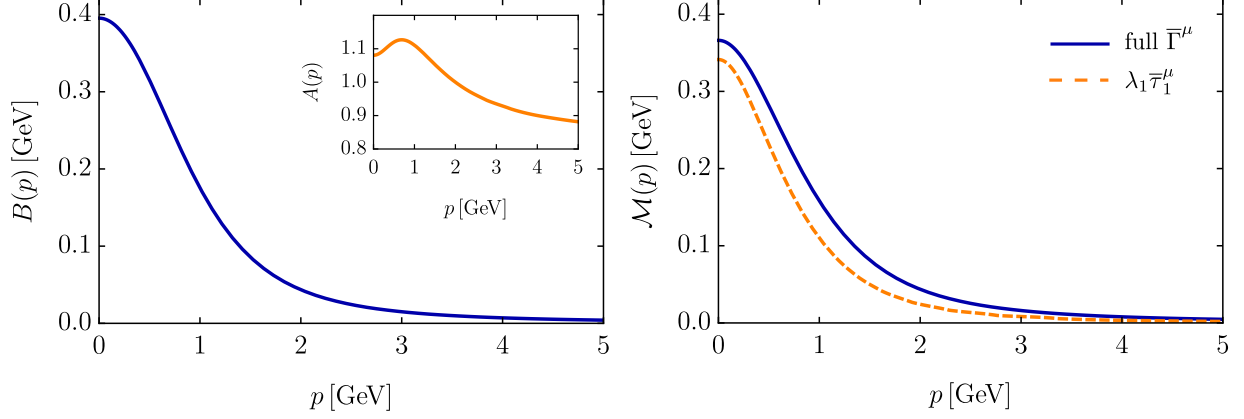


FIG. 9. Results of the quark gap-equation solution. **Left panel:** The quark dressing function  $B(p)$ , with the corresponding dressing  $A(p)$  displayed in the inset. **Right panel:** The constituent quark mass function  $\mathcal{M}(p) = B(p)/A(p)$ , shown together with the result obtained when retaining only the classical part of the quark–gluon vertex.

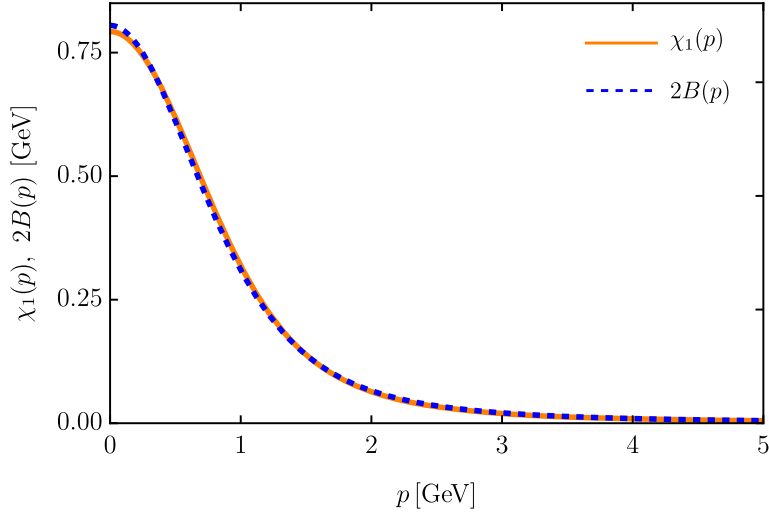


FIG. 10. Numerical confirmation of the relation  $\chi_1(p) = 2B(p)$ , Eq. (2.14), which follows from the axial WTI. The relation is satisfied within the numerical accuracy of the (two-) loop integrals, *i.e.*, one percent or better.

$B(p)$ ; their accompanying tensors,  $\bar{\tau}_5^\mu$  and  $\bar{\tau}_7^\mu$ , are annihilated in the projection appearing in the first line of Eq. (2.6). Nevertheless, these form factors contribute to  $\mathcal{M}(p)$  through  $A(p)$ .

## D. BSE

For the numerical solution of the BSE given by Eqs. (5.13) and (5.14) we adopt standard techniques, discretizing the momentum integrals using Gauss-Legendre and Gauss-Chebyshev quadratures, and reformulating the equation as an eigenvalue problem of the form [31, 89, 96, 97]

$$\lambda(P^2) \chi_1(p) = \mathbf{K}(P^2) \chi_1(p). \quad (6.7)$$

$\mathbf{K}(P^2)$  denotes the interaction kernel, which in our case is composed of the three diagrams shown in Fig. 5. In general, the eigenvalue  $\lambda(P^2)$  depends continuously on the total momentum, and the mass  $M$  of the bound state is determined from the condition  $\lambda(P^2 = -M^2) = 1$ . The dominant eigenvalue and its corresponding eigenvector are obtained numerically using iterative eigensolvers, such as the “power method” or the “Arnoldi iteration”, which ensure stable convergence [96, 98, 99]. As already mentioned, in the present analysis we restrict ourselves to the case of the chiral limit, where the current quark mass  $m$  vanishes, and consequently, the pion is exactly massless, corresponding to the condition  $\lambda(P^2 = 0) = 1$ .

As may be seen in Fig. 10, the pion BSA,  $\chi_1(p)$ , obtained from this analysis, satisfies at a high degree of accuracy (better than 1%) the symmetry-induced relation given in Eq. (2.14). This result is of central importance, because it constitutes a clear numerical confirmation of the symmetry-preserving nature of the entire approach.

The individual contributions of the three diagrams to the eigenvalue  $\lambda$  are displayed in the left panel of Fig. 11: the “dressed RL” diagram provides approximately 66% of the total value, the “quantum” diagram accounts for about 33%, while the “crossed” diagram contributes around 1%. However, even though the “crossed” contributes slightly, its rôle is crucial in maintaining the exact realization of the chiral solution. In particular, given that the BSE is an eigenvalue problem, even a small deviation from unity, for example,  $\lambda(0) = 0.99$  instead of  $\lambda(0) = 1$  would correspond to a large mass shift, thus invalidating the masslessness of the pion. Therefore, all three diagrams are indispensable: the precise value  $\lambda(P^2 = 0) = 1$  arises only when their combined contributions are taken into account. Neglecting any of them distorts this delicate balance, thwarting the proper emergence of the Nambu-Goldstone boson associated with the dynamical breaking of the chiral symmetry.

As a consistency check, once the amplitude  $\chi_1(p)$  is obtained from the eigenvalue problem in Eq. (6.7), we substitute it back into the full integral equation Eq. (5.14). This allows us

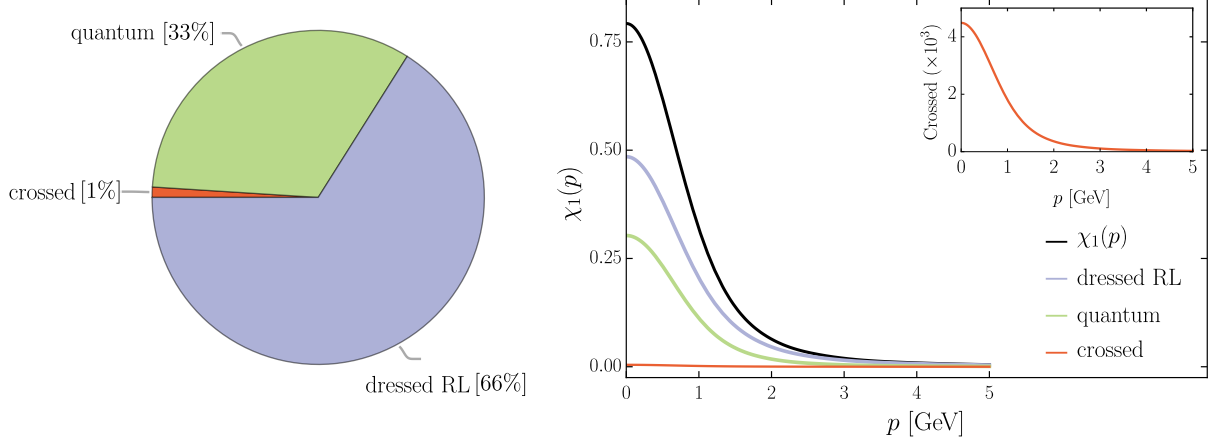


FIG. 11. **Left panel:** Individual eigenvalue contributions from each diagram entering into the full BSE solution in Eq. (5.14). **Right panel:** Full pion BSA,  $\chi_1(p)$ , together with the individual contributions stemming from each diagram.

to evaluate separately the contribution of each diagram to the total BSA (right panel of Fig. 11). We find that the sum of these three individual contributions reconstructs the original solution with high numerical accuracy, confirming the internal consistency of our implementation.

### E. Varying the $V(q)$

In order to probe the robustness of our results and the internal consistency of the truncation underlying the coupled SDE-BSE framework, we have implemented variations around the central fit of  $V(q)$ , shown in the left panel of Fig. 12, and have tested the persistence of the key relation  $\chi_1(p) = 2B(p)$ , see Eq. (2.14). As explained earlier, from the theoretical point of view, the validity of this relation does not hinge on the specific form of the function  $V(q)$ ; the only requirement is that the latter depends on a single variable, which is identified with the gluon momentum entering into the specific quark-gluon vertex.

The variations implemented on  $V(q)$  induce corresponding changes to the vertex form factors  $\lambda_i$ , which then propagate to the quark gap equation and the BSE. Importantly, in all cases considered, the corresponding eigenvalue  $\lambda(P^2)$  remains stable and continues to satisfy the condition  $\lambda(P^2 = 0) = 1$ . As a result, one obtains a sequence of pairs  $\{\chi_1(p), B(p)\}$ , which, even though they are different from one another, have a key property in common:

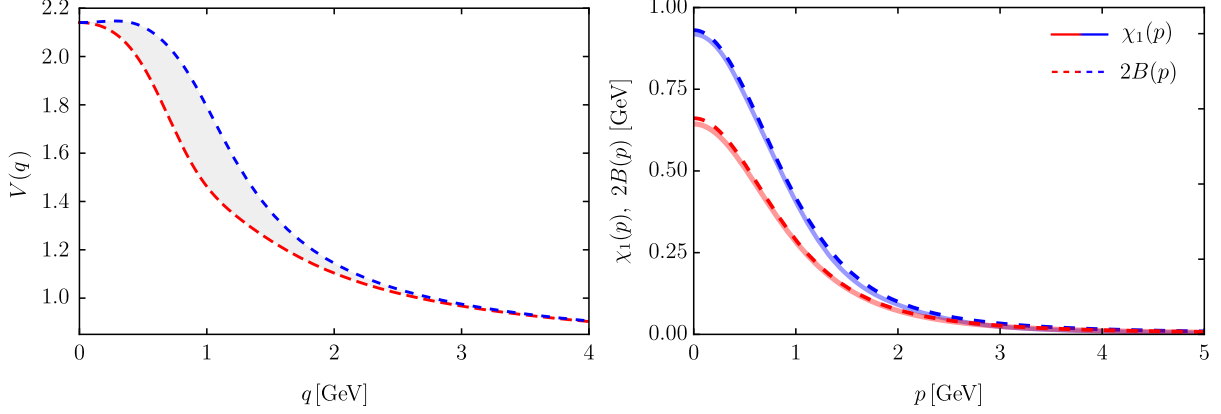


FIG. 12. **Left panel:** Variations around the central parametrization of  $V(q)$  employed to assess the robustness of the calculation. **Right panel:** Resulting pion BSAs obtained from these variations, shown together with  $2B(p)$ . The blue and red curves correspond to the upper and lower variations of the fit  $V(q)$ , respectively.

they fulfil the WTI-induced constraint  $\chi_1(p) = 2B(p)$  at a high level of accuracy (1% discrepancy), see right panel of Fig. 12. We therefore conclude that the resulting massless pion is not a contingent feature of a particular parametrization, but a robust consequence of the self-consistent SDE-BSE truncation.

## VII. DISCUSSION AND CONCLUSIONS

We have presented a detailed numerical treatment of the dynamical equations within the recently developed approach to the physics of mesons [1]. We concentrated on the special case of the chiral limit with a massless pion. The analysis goes significantly beyond the standard RL treatments, employing fully-dressed quark-gluon vertices in both the gap equation and the pion BSE. This quark-gluon vertex is obtained from an approximate form of the standard SDE within the 3PI formalism, and contains all eight transverse form factors with their full momentum dependence. The respective truncation and subsequent renormalization of the BSE kernel leads to a dynamical equation for the pion amplitude that consists of three special diagrams, two one-loop dressed, denominated as “dressed RL” and “quantum”, and a two-loop dressed graph, coined “crossed”. The symmetry-preserving character of the truncation was confirmed explicitly by checking of the pivotal relation  $\chi_1(p) = 2B(p)$ . It is satisfied exactly within the numerical precision of the respective (two-) loop integrals, that

is, a precision of  $\lesssim 1\%$  in the entire range of momenta, see [Fig. 10](#).

The numerical error originates mainly from the treatment of the two-loop contribution (“crossed” diagram) in the BSE kernel, whose evaluation is considerably more demanding than the one-loop terms. In particular, the resolution of the integration grid and the need to balance numerical cost with stability introduce a controlled uncertainty at very small momenta. A refined grid sampling would systematically reduce this effect, and will be implemented in the near future. In any case, the present level of agreement already confirms that the truncation preserves the axial symmetry.

In addition, the BSE eigenvalue was found to be equal to unity to four significant figures, and the individual contributions of the aforementioned three graphs to its composition (66%, 33%, and 1%, respectively) was ascertained. From the technical point of view, it is worth stressing that the present study deals for the first time with the evaluation of the two-loop diagram (“crossed”); in particular, even though the relevance of this graph had been briefly alluded in [\[8\]](#), its numerical treatment has never been reported.

In order to extend the above analysis beyond the chiral limit, and obtain the physical masses of the pion and other mesons, the general theoretical framework developed in [\[1\]](#) must be generalized to the case of nonvanishing quark masses. In addition, and more importantly, several of the key equations must be evaluated for complex values of the momenta. The need for such a generalization may already be seen at the level of the meson BSE, whose incoming momentum must satisfy the condition  $P^2 = -M^2$ , where  $M$  is the mass of the meson in question. Therefore, according to the standard parametrization [\[96\]](#), one sets  $P^\mu = (0, 0, 0, iM)$  inside the BSE, and, as a result, knowledge of the BSE ingredients beyond the real Euclidean axis is needed. The need to extend the treatment of the gap equation to accommodate complex momenta is already known from the standard RL studies, see, *e.g.*, [\[31, 37–46, 48, 53–55, 96\]](#); however, the present formulation requires, in addition, the corresponding generalization on the complex plane of the form factors that compose the quark-gluon vertex. The study of the structure of the quark-gluon vertex for complex momenta is naturally integrated in the general exploration of QCD correlation functions on the complex plane, which is being implemented using a variety of approaches, such as [\[100–114\]](#). We hope to report progress in this direction in the near future.

## ACKNOWLEDGMENTS

The work of M.N.F. is supported by the National Natural Science Foundation of China (grants 12135007 and W2433021). A.S.M., J.M.M. and J.P. are funded by the Spanish MICINN grants PID2020-113334GB-I00 and PID2023-151418NB-I00, the Generalitat Valenciana grant CIPROM/2022/66, and CEX2023-001292-S by MCIU/AEI. J.M.P. is funded by the Deutsche Forschungsgemeinschaft (DFG, German Research Foundation) under Germany's Excellence Strategy EXC 2181/1 - 390900948 (the Heidelberg STRUCTURES Excellence Cluster) and the Collaborative Research Centre SFB 1225 - 273811115 (ISOQUANT).

## Appendix A: Diagrammatics of Eq. (2.15).

In this appendix we demonstrate the validity of Eq. (2.15) when the approximations and truncations described in the main text are implemented; the demonstration proceeds directly at the level of the diagrams that compose both sides of Eq. (2.15).

When the vertex  $G_5^{\mu\nu}$  is approximated by the sum of the graphs  $d_1$ ,  $d_2$ , and  $d_3$  in Fig. 3A, the l.h.s. of the WTI in Eq. (2.15) is given by

$$\lim_{P \rightarrow 0} P_\mu G_5^{\mu\nu}(P, q, p_2, -q_1) = d_{1\chi}^\nu + d_{2\chi}^\nu + d_{3\chi}^\nu, \quad (\text{A1})$$

with (see Fig. 13)

$$\begin{aligned} d_{1\chi}^\nu &= -ic_a \int_k \gamma^\beta c(p+k+q) \chi_1(p+k+q) \gamma^\nu S(-p-k) \gamma^\alpha \Delta_{\alpha\beta}(k) V^2(k) V(q) \gamma_5, \\ d_{2\chi}^\nu &= ic_a \int_k \gamma^\beta S(p+k+q) \gamma^\nu c(p+k) \chi_1(p+k) \gamma^\alpha \Delta_{\alpha\beta}(k) V^2(k) V(q) \gamma_5, \\ d_{3\chi}^\nu &= ic_b \int_k \gamma^\beta c(p+k) \chi_1(p+k) \gamma^\alpha \Gamma^{\nu\rho\delta}(q, -k, k') \Delta_{\alpha\rho}(k) V(k) \Delta_{\delta\beta}(k') V(k') \gamma_5. \end{aligned} \quad (\text{A2})$$

Since the r.h.s. of Eq. (2.15) is given by the even component of the quark-gluon vertex graphs  $c_1^\nu$  and  $c_2^\nu$  in Fig. 3B, equating both sides yields

$$d_{1\chi}^\nu + d_{2\chi}^\nu + d_{3\chi}^\nu = 2i(c_{1,2}^\nu + c_{2,2}^\nu) \gamma_5, \quad (\text{A3})$$

where the rightmost subscript “2” in  $c_{1,2}^\nu$  and  $c_{2,2}^\nu$  indicates the part of the diagrams that contain an even number of Dirac  $\gamma$  matrices. In fact, the obvious separation of graphs into

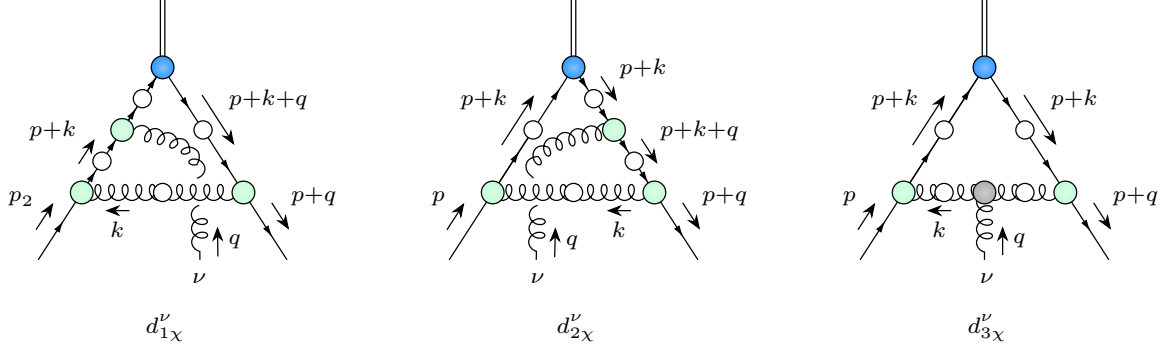


FIG. 13. Diagrammatic representation of the three contributions to the pole part of  $G_5^{\mu\nu}$ .

Abelian (no three-gluon vertex) and non-Abelian (three-gluon vertex) reduces Eq. (A3) to two simpler relations, namely

$$d_{1\chi}^\nu + d_{2\chi}^\nu = 2ic_{1,2}^\nu \gamma_5, \quad d_{3\chi}^\nu = 2ic_{2,2}^\nu \gamma_5, \quad (\text{A4})$$

which we proceed to prove.

We now introduce the following diagrammatic representation for the components of the quark propagator, see Eq. (2.6b),

$$\begin{aligned} a(p)\not{p} = c(p)A(p)\not{p} &= \frac{p}{\longrightarrow} \longrightarrow \triangle \longrightarrow, \\ b(p) &= c(p)B(p) = \frac{p}{\longrightarrow} \longrightarrow \times \longrightarrow, \end{aligned} \quad (\text{A5})$$

which is useful in the ensuing analysis.

We start considering the non-Abelian diagram  $c_2^\nu$ , Eq. (3.3), and determine its even component,

$$\begin{aligned} c_{2,2}^\nu &= c_b \int_k [\gamma^\beta S(p+k) \gamma^\alpha]_{\text{even}} \Gamma^{\nu\rho\delta}(q, -k, k') \Delta_{\alpha\rho}(k) V(k) \Delta_{\delta\beta}(k') V(k') \\ &= c_b \kappa_b \int_k \gamma^\beta b(p+k) \gamma^\alpha \Gamma^{\nu\rho\delta}(q, -k, k') \Delta_{\alpha\rho}(k) V(k) \Delta_{\delta\beta}(k') V(k') \\ &= \frac{c_b}{2} \int_k \gamma^\beta c(p+k) \chi_1(p+k) \gamma^\alpha \Gamma^{\nu\rho\delta}(q, -k, k') \Delta_{\alpha\rho}(k) V(k) \Delta_{\delta\beta}(k') V(k') \\ &= -\frac{i}{2} d_{3\chi}^\nu \gamma_5, \end{aligned} \quad (\text{A6})$$

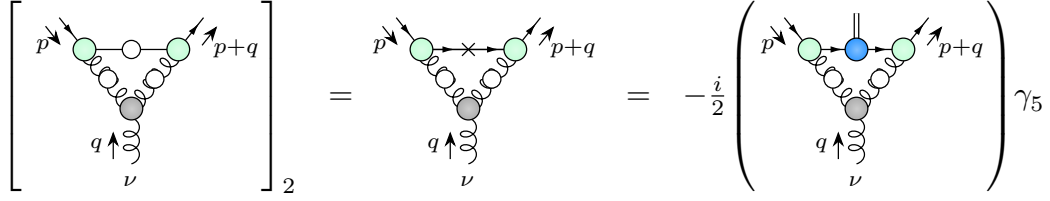


FIG. 14. Diagrammatic realization of Eq. (A6).

*i.e.*, the relation given in Eq. (A4). With the aid of the symbols introduced in Eq. (A5), this identity may be expressed diagrammatically as shown in Fig. 14.

The Abelian case proceeds in the same way, but is algebraically slightly more involved. To begin with, an important cancellation takes place when  $d_{1,\chi}$  and  $d_{2,\chi}$  are summed. In particular, defining

$$\mathcal{T}_{\alpha\beta}(k, q) = \Delta_{\alpha\beta}(k)V^2(k)V(q), \quad \ell = p + k + q, \quad (\text{A7})$$

we have

$$\begin{aligned} d_{1\chi} + d_{2\chi} &= ic_a \int_k \gamma^\beta S(\ell) \gamma^\nu c(p+k) \chi_1(p+k) \gamma^\alpha \mathcal{T}_{\alpha\beta}(k, q) \gamma_5 \\ &\quad - ic_a \int_k \gamma^\beta c(\ell) \chi_1(\ell) \gamma^\nu S(-p-k) \gamma^\alpha \mathcal{T}_{\alpha\beta}(k, q) \gamma_5 \\ &= ic_a \int_k \gamma^\beta S(\ell) \gamma^\nu c(p+k) \chi_1(p+k) \gamma^\alpha \mathcal{T}_{\alpha\beta}(k, q) \gamma_5 \\ &\quad - ic_a \int_k \gamma^\beta c(\ell) \chi_1(\ell) \gamma^\nu S(-p-k) \gamma^\alpha \mathcal{T}_{\alpha\beta}(k, q) \gamma_5 \\ &= ic_a \int_k \gamma^\beta a(\ell) \not{\ell} \gamma^\nu c(p+k) \chi_1(p+k) \gamma^\alpha \mathcal{T}_{\alpha\beta}(k, q) \gamma_5 \\ &\quad + ic_a \int_k \gamma^\beta c(\ell) \chi_1(\ell) \gamma^\nu a(\ell) \not{\ell} \gamma^\alpha \mathcal{T}_{\alpha\beta}(k, q) \gamma_5 \\ &\quad + ic_a \int_k \gamma^\beta b(\ell) \gamma^\nu c(p+k) \chi_1(p+k) \gamma^\alpha \mathcal{T}_{\alpha\beta}(k, q) \gamma_5 \\ &\quad - ic_a \int_k \gamma^\beta c(\ell) \chi_1(\ell) \gamma^\nu b(p+k) \gamma^\alpha \mathcal{T}_{\alpha\beta}(k, q) \gamma_5. \end{aligned} \quad (\text{A8})$$



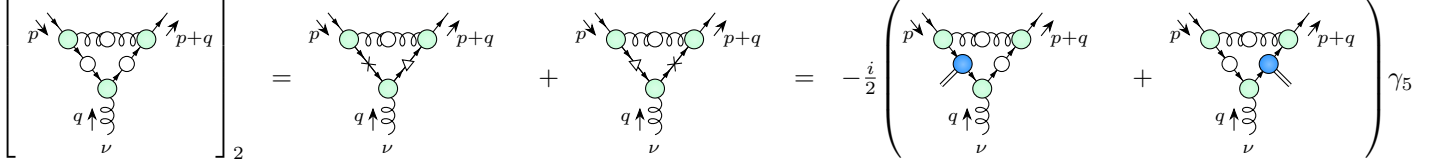


FIG. 15. Diagrammatic realization of Eq. (A10).

The announced cancellation takes place between the last two terms, once the first relation in Eq. (2.14),  $2b(p) = c(p)\chi_1(p)$ , has been invoked, leaving us with

$$\begin{aligned}
 d_{1\chi} + d_{2\chi} &= ic_a \int_k \gamma^\beta a(\ell) \not{\ell} \gamma^\nu c(p+k) \chi_1(p+k) \gamma^\alpha \mathcal{T}_{\alpha\beta}(k, q) \\
 &\quad + ic_a \int_k \gamma^\beta c(\ell) \chi_1(\ell) \gamma^\nu a(p+k) \not{p} \gamma^\alpha \mathcal{T}_{\alpha\beta}(k, q) \gamma_5. \tag{A9}
 \end{aligned}$$

Consider now the even part of the diagram  $c_1^\nu$ , namely

$$\begin{aligned}
 c_{1,2}^\nu &= c_a \int_k [\gamma^\beta S(\ell) \gamma^\nu S(p+k) \gamma^\alpha]_{\text{even}} \mathcal{T}_{\alpha\beta}(k, q) \\
 &= c_a \int_k \gamma^\beta a(\ell) \not{\ell} \gamma^\nu b(p+k) \gamma^\alpha \mathcal{T}_{\alpha\beta}(k, q) \\
 &\quad + c_a \int_k \gamma^\beta b(\ell) \gamma^\nu a(p+k) (\not{p} + \not{k}) \gamma^\alpha \mathcal{T}_{\alpha\beta}(k, q) \\
 &= \frac{c_a}{2} \int_k \gamma^\beta a(\ell) \not{\ell} \gamma^\nu c(p+k) \chi_1(p+k) \gamma^\alpha \mathcal{T}_{\alpha\beta}(k, q) \\
 &\quad + \frac{c_a}{2} \int_k \gamma^\beta c(\ell) \chi_1(\ell) \gamma^\nu a(p+k) (\not{p} + \not{k}) \gamma^\alpha \mathcal{T}_{\alpha\beta}(k, q) \\
 &= -\frac{i}{2} (d_{1\chi}^\nu + d_{2\chi}^\nu) \gamma_5, \tag{A10}
 \end{aligned}$$

which is the first relation in Eq. (A4); in the last step, Eq. (A9) was used. The final result may be depicted as shown in Fig. 15.

## Appendix B: An interesting identity

In this appendix we derive an approximate integral constraint relating the odd and even components of the quark-gluon vertex,  $\Gamma_1^\mu(q, r, -p)$  and  $\Gamma_2^\mu(q, r, -p)$ , respectively. This con-

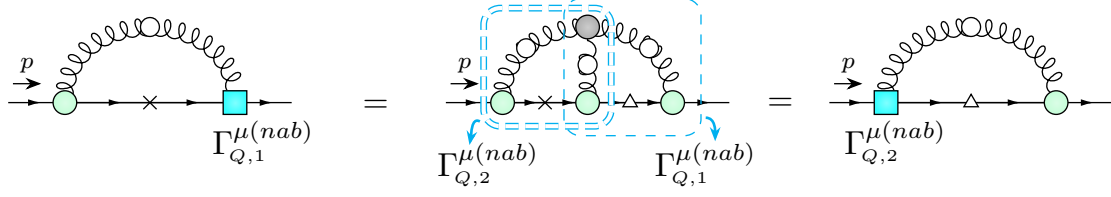


FIG. 16. Diagrammatic demonstration of the identity Eq. (B2).

straint stems from an identity relating the odd and even parts of the non-Abelian diagram in the quark-gluon vertex SDE of Fig. 3B.

To derive the identity of interest, consider the expression

$$i \int_q b(q') \text{Tr} \left[ \Gamma_1^{\sigma(nab)}(-q, q', -p) V^\nu(q) \right] \Delta_{\nu\sigma}(q), \quad (\text{B1})$$

corresponding to the diagram on the l.h.s. of Fig. 16. The superscript “*nab*” labels de non-Abelian contribution to the quark-gluon vertex. Note that, up to an overall prefactor, this diagram is a contribution to the renormalized gap equation. Then, using for  $\Gamma_1^{\sigma(nab)}$  the explicit SDE diagram ( $c_2$  in Fig. 3B), we obtain the two-loop diagram in the center of Fig. 16. At this point, the loop on the left part of the two-loop diagram, highlighted by a double-dashed line, is immediately recognized as  $\Gamma_2^{\nu(nab)}$ . Thus, we obtain the following identity for the non-Abelian contribution

$$t_1^{(nab)}(p) = t_2^{(nab)}(p), \quad (\text{B2})$$

where

$$\begin{aligned} t_1^{(nab)}(p) &:= i \int_q b(q') \text{Tr} \left[ \Gamma_1^{\sigma(nab)}(-q, q', -p) V^\nu(q) \right] \Delta_{\nu\sigma}(q), \\ t_2^{(nab)}(p) &:= i \int_q a(q') \text{Tr} \left[ V^\sigma(q) \not{q}' \Gamma_2^{\nu(nab)}(q, p, -q') \right] \Delta_{\nu\sigma}(q). \end{aligned} \quad (\text{B3})$$

Evidently, repeating this argument but placing  $\Gamma_1^{\sigma(nab)}$  on the quark leg instead of the antiquark in Fig. 16, leads to another identity

$$\tilde{t}_1^{(nab)}(p) = \tilde{t}_2^{(nab)}(p), \quad (\text{B4})$$

with

$$\begin{aligned} \tilde{t}_1^{(nab)}(p) &:= i \int_q b(q') \text{Tr} \left[ V^\nu(q) \Gamma_1^{\sigma(nab)}(q, p, -q') \right] \Delta_{\nu\sigma}(q), \\ \tilde{t}_2^{(nab)}(p) &:= i \int_q a(q') \text{Tr} \left[ \Gamma_2^{\nu(nab)}(-q, q', -p) \not{q}' V^\sigma(q) \right] \Delta_{\nu\sigma}(q). \end{aligned} \quad (\text{B5})$$

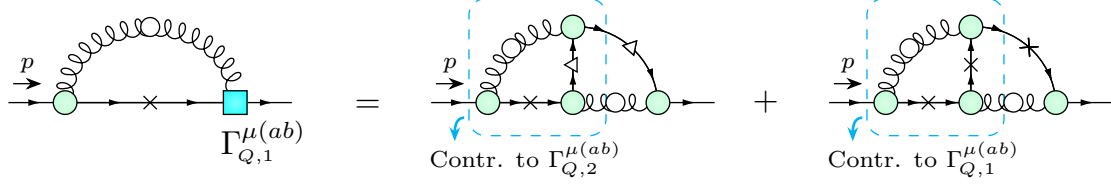


FIG. 17. Diagrammatic representation of the integral in B7.

Invoking the charge conjugation transformation of the vertex (see, *e.g.*, Eq. (2.7) of [60]) and elementary properties of the trace, it is straightforward to show that

$$\tilde{t}_1^{(nab)}(p) = t_1^{(nab)}(p). \quad (\text{B6})$$

Note that a similar result *does not* hold for the Abelian contribution, as shown diagrammatically in Fig. 17. In this case, the integral analogous to the l.h.s. of Eq. (B2), namely

$$i \int_q b(q') \text{Tr} \left[ \Gamma_1^{\sigma(ab)}(-q, q', -p) V^\nu(q) \right] \Delta_{\nu\sigma}(q), \quad (\text{B7})$$

with “ $ab$ ” labeling the Abelian part of the quark-gluon vertex, corresponds to the diagram on the left of Fig. 17. Using the SDE diagrams of Fig. 3B for  $\Gamma_{1,Q}^{\sigma(ab)}$ , we get the two-loop diagrams on the right of that figure. There, the first diagram on the right can be seen to furnish a contribution to  $\Gamma_2^{\nu(ab)}$ . However, the second diagram generates a contribution to  $\Gamma_1^{\nu(ab)}$  instead. Thus, the sum of the two terms enclosed in the blue boxes does not furnish the full  $\Gamma_2^{\nu(ab)}$ .

Nevertheless, the quark-gluon vertex is known to be dominated by its non-Abelian diagram [12, 60]. Consequently, Eq. (B2) should hold approximately for the quantum part of the vertex, *i.e.*,

$$t_1(p) \approx t_2(p), \quad (\text{B8})$$

where

$$\begin{aligned} t_1(p) &:= i \int_q b(q') \text{Tr} \left[ \Gamma_{Q,1}^\sigma(-q, q', -p) V^\nu(q) \right] \Delta_{\nu\sigma}(q), \\ t_2(p) &:= i \int_q a(q') \text{Tr} \left[ V^\sigma(q) \not{q}' \Gamma_{Q,2}^\nu(q, p, -q') \right] \Delta_{\nu\sigma}(q). \end{aligned} \quad (\text{B9})$$

Then, using the inputs described in Sec. VI for  $a(p)$ ,  $b(p)$ , and  $V(p)$ , we compute the  $\Gamma_i^{\sigma(nab)}$ , for  $i = 1, 2$ , and use the latter to evaluate the  $t_i^{(nab)}(p)$  through Eq. (B3). The results are shown on the left panel of Fig. 18. There, the relative error,  $[t_1^{(nab)}(p) - t_2^{(nab)}(p)]/t_1^{(nab)}(p)$ ,

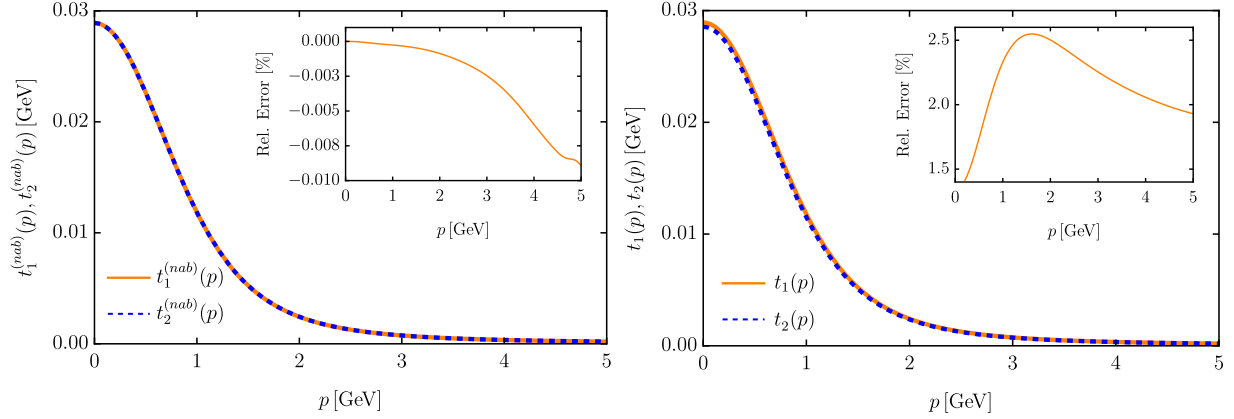


FIG. 18. **Left panel:** Integrals  $t_1^{(nab)}(p)$  (orange continuous) and  $t_2^{(nab)}(p)$  (blue dashed), appearing in the identity of Eq. (B2), and the relative difference between them (inset). **Right panel:** Analogous terms,  $t_1(p)$  (orange continuous) and  $t_2(p)$  (blue dashed), including the Abelian contribution. In this case, the relative difference is not compatible with zero. Nevertheless, Eq. (B8) holds within 2.5%.

which is less than  $10^{-4}$ , is shown as an inset. Since the numerical precision of our numerical calculations is known to be of that same order, this error is compatible with zero. Thus, Eq. (B2) is verified.

Next, we quantify the precision to which Eq. (B8) is satisfied when both Abelian and non-Abelian contributions are included in the vertex SDE. The results for the  $t_i(p)$  are shown on the right panel of Fig. 18, and are barely distinguishable from each other, as well as from the  $t_i^{(nab)}$  shown on the left panel, confirming that the non-Abelian contribution dominates the quark-gluon vertex. As a result, Eq. (B8) is satisfied within 2.5%, as seen on the inset.

- 
- [1] A. S. Miramontes, J. M. Morgado, J. Papavassiliou, and J. M. Pawłowski, *Eur. Phys. J. C* **85**, 1055 (2025).
  - [2] H. Munczek, *Phys. Rev. D* **52**, 4736 (1995).
  - [3] H. H. Matevosyan, A. W. Thomas, and P. C. Tandy, *Phys. Rev. C* **75**, 045201 (2007).
  - [4] C. S. Fischer, D. Nickel, and J. Wambach, *Phys. Rev. D* **76**, 094009 (2007).
  - [5] C. S. Fischer and R. Williams, *Phys. Rev. D* **78**, 074006 (2008).
  - [6] C. S. Fischer and R. Williams, *Phys. Rev. Lett.* **103**, 122001 (2009).

- [7] L. Chang and C. D. Roberts, [Phys. Rev. Lett. \*\*103\*\*, 081601 \(2009\)](#).
- [8] H. Sanchis-Alepuz and R. Williams, [J. Phys. Conf. Ser. \*\*631\*\*, 012064 \(2015\)](#).
- [9] R. Williams, [Eur. Phys. J. \*\*A51\*\*, 57 \(2015\)](#).
- [10] W. Heupel, T. Goecke, and C. S. Fischer, [Eur. Phys. J. \*\*A50\*\*, 85 \(2014\)](#).
- [11] H. Sanchis-Alepuz, C. S. Fischer, and S. Kubrak, [Phys. Lett. B \*\*733\*\*, 151 \(2014\)](#).
- [12] R. Williams, C. S. Fischer, and W. Heupel, [Phys. Rev. \*\*D93\*\*, 034026 \(2016\)](#).
- [13] H. Sanchis-Alepuz and R. Williams, [Phys. Lett. \*\*B749\*\*, 592 \(2015\)](#).
- [14] D. Binosi, L. Chang, J. Papavassiliou, S.-X. Qin, and C. D. Roberts, [Phys. Rev. \*\*D93\*\*, 096010 \(2016\)](#).
- [15] R. Williams, [Phys. Lett. B \*\*798\*\*, 134943 \(2019\)](#).
- [16] Á. S. Miramontes, H. Sanchis Alepuz, and R. Alkofer, [Phys. Rev. D \*\*103\*\*, 116006 \(2021\)](#).
- [17] N. Santowsky, G. Eichmann, C. S. Fischer, P. C. Wallbott, and R. Williams, [Phys. Rev. D \*\*102\*\*, 056014 \(2020\)](#).
- [18] Á. S. Miramontes, R. Alkofer, C. S. Fischer, and H. Sanchis-Alepuz, [Phys. Lett. B \*\*833\*\*, 137291 \(2022\)](#).
- [19] F. Gao, A. S. Miramontes, J. Papavassiliou, and J. M. Pawłowski, [Phys. Lett. B \*\*863\*\*, 139384 \(2025\)](#).
- [20] A. S. Miramontes, G. Eichmann, and R. Alkofer, [Phys. Lett. B \*\*868\*\*, 139659 \(2025\)](#).
- [21] W.-j. Fu, C. Huang, J. M. Pawłowski, Y.-y. Tan, and L.-j. Zhou, [Phys. Rev. D \*\*112\*\*, 054047 \(2025\)](#), [arXiv:2502.14388 \[hep-ph\]](#).
- [22] M. Q. Huber, C. S. Fischer, and H. Sanchis-Alepuz, [Eur. Phys. J. C \*\*85\*\*, 859 \(2025\)](#), [arXiv:2503.03821 \[hep-ph\]](#).
- [23] A. S. Miramontes, J. Papavassiliou, and J. M. Pawłowski, [arXiv:2508.20631 \[hep-ph\] \(2025\)](#).
- [24] R. Alkofer and L. von Smekal, [Phys. Rept. \*\*353\*\*, 281 \(2001\)](#).
- [25] P. Maris and C. D. Roberts, [Int. J. Mod. Phys. \*\*E12\*\*, 297 \(2003\)](#).
- [26] C. S. Fischer, [J. Phys. G \*\*32\*\*, R253 \(2006\)](#).
- [27] D. Binosi and J. Papavassiliou, [Phys. Rept. \*\*479\*\*, 1 \(2009\)](#).
- [28] A. Maas, [Phys. Rept. \*\*524\*\*, 203 \(2013\)](#).
- [29] A. Bashir, L. Chang, I. C. Cloet, B. El-Bennich, Y.-X. Liu, *et al.*, [Commun. Theor. Phys. \*\*58\*\*, 79 \(2012\)](#).
- [30] I. C. Cloet and C. D. Roberts, [Prog. Part. Nucl. Phys. \*\*77\*\*, 1 \(2014\)](#).

- [31] G. Eichmann, H. Sanchis-Alepuz, R. Williams, R. Alkofer, and C. S. Fischer, [Prog. Part. Nucl. Phys. \*\*91\*\*, 1 \(2016\)](#).
- [32] C. S. Fischer, [Prog. Part. Nucl. Phys. \*\*105\*\*, 1 \(2019\)](#).
- [33] M. Q. Huber, [Phys. Rept. \*\*879\*\*, 1 \(2020\)](#).
- [34] M. N. Ferreira and J. Papavassiliou, [Particles \*\*6\*\*, 312 \(2023\)](#).
- [35] A. Bender, W. Detmold, C. Roberts, and A. W. Thomas, [Phys. Rev. \*\*C65\*\*, 065203 \(2002\)](#).
- [36] P. Maris and P. C. Tandy, [Phys. Rev. \*\*C60\*\*, 055214 \(1999\)](#).
- [37] P. Maris and P. C. Tandy, [Phys. Rev. \*\*C 61\*\*, 045202 \(2000\)](#).
- [38] R. Alkofer, P. Watson, and H. Weigel, [Phys. Rev. \*\*D 65\*\*, 094026 \(2002\)](#).
- [39] G. Eichmann, R. Alkofer, I. C. Cloet, A. Krassnigg, and C. D. Roberts, [Phys. Rev. \*\*C 77\*\*, 042202 \(2008\)](#).
- [40] S.-x. Qin, L. Chang, Y.-x. Liu, C. D. Roberts, and D. J. Wilson, [Phys. Rev. \*\*C84\*\*, 042202 \(2011\)](#).
- [41] T. Hilger, C. Popovici, M. Gomez-Rocha, and A. Krassnigg, [Phys. Rev. \*\*D 91\*\*, 034013 \(2015\)](#).
- [42] W. Heupel, G. Eichmann, and C. S. Fischer, [Phys. Lett. \*\*B 718\*\*, 545 \(2012\)](#).
- [43] G. Eichmann, C. S. Fischer, and W. Heupel, [Phys. Lett. \*\*B 753\*\*, 282 \(2016\)](#).
- [44] T. Hilger, M. Gomez-Rocha, and A. Krassnigg, [Phys. Rev. \*\*D 91\*\*, 114004 \(2015\)](#).
- [45] B. El-Bennich, G. Krein, E. Rojas, and F. E. Serna, [Few Body Syst. \*\*57\*\*, 955 \(2016\)](#).
- [46] F. F. Mojica, C. E. Vera, E. Rojas, and B. El-Bennich, [Phys. Rev. \*\*D 96\*\*, 014012 \(2017\)](#).
- [47] K. Raya, M. A. Bedolla, J. J. Cobos-Martínez, and A. Bashir, [Few Body Syst. \*\*59\*\*, 133 \(2018\)](#).
- [48] E. Weil, G. Eichmann, C. S. Fischer, and R. Williams, [Phys. Rev. \*\*D 96\*\*, 014021 \(2017\)](#).
- [49] F. E. Serna, B. El-Bennich, and G. Krein, [Phys. Rev. \*\*D 96\*\*, 014013 \(2017\)](#).
- [50] L. X. Gutiérrez-Guerrero, G. Paredes-Torres, and A. Bashir, [Phys. Rev. \*\*D 104\*\*, 094013 \(2021\)](#).
- [51] R. J. Hernández-Pinto, L. X. Gutiérrez-Guerrero, A. Bashir, M. A. Bedolla, and I. M. Higuera-Angulo, [Phys. Rev. \*\*D 107\*\*, 054002 \(2023\)](#).
- [52] R. J. Hernández-Pinto, L. X. Gutiérrez-Guerrero, M. A. Bedolla, and A. Bashir, [Phys. Rev. \*\*D 110\*\*, 114015 \(2024\)](#).
- [53] M. Chen and L. Chang, [Chin. Phys. \*\*C 43\*\*, 114103 \(2019\)](#).
- [54] L. Chang and M. Ding, [Phys. Rev. \*\*D 103\*\*, 074001 \(2021\)](#).
- [55] Y.-Z. Xu, [JHEP \*\*2024\*\* \(7\), 118](#).

- [56] Y.-Z. Xu, [Phys. Rev. D \*\*111\*\*, 114012 \(2025\)](#).
- [57] Y. Z. Xu, K. Raya, J. Rodríguez-Quintero, and J. Segovia, [Phys. Rev. D \*\*110\*\*, 054031 \(2024\)](#).
- [58] L. Albino, G. Paredes-Torres, K. Raya, A. Bashir, and J. Segovia, [Phys. Rev. D \*\*112\*\*, 074015 \(2025\)](#).
- [59] R. Alkofer, C. S. Fischer, F. J. Llanes-Estrada, and K. Schwenzer, [Annals Phys. \*\*324\*\*, 106 \(2009\)](#).
- [60] A. C. Aguilar, M. N. Ferreira, B. M. Oliveira, J. Papavassiliou, and G. T. Linhares, [Eur. Phys. J. C \*\*84\*\*, 1231 \(2024\)](#).
- [61] F. Gao, J. Papavassiliou, and J. M. Pawłowski, [Phys. Rev. D \*\*103\*\*, 094013 \(2021\)](#).
- [62] E. E. Salpeter and H. A. Bethe, [Phys. Rev. \*\*84\*\*, 1232 \(1951\)](#).
- [63] M. Gell-Mann and F. Low, [Phys. Rev. \*\*84\*\*, 350 \(1951\)](#).
- [64] H. A. Bethe and E. E. Salpeter, Quantum mechanics of one- and two-electron systems, in [Atoms I / Atome I](#) (Springer Berlin Heidelberg, Berlin, Heidelberg, 1957) pp. 88–436.
- [65] N. Nakanishi, [Prog. Theor. Phys. Suppl. \*\*43\*\*, 1 \(1969\)](#).
- [66] P. Jain and H. J. Munczek, [Phys. Rev. D \*\*48\*\*, 5403 \(1993\)](#).
- [67] C. S. Fischer and R. Alkofer, [Phys. Rev. \*\*D67\*\*, 094020 \(2003\)](#).
- [68] A. C. Aguilar and J. Papavassiliou, [Phys. Rev. \*\*D83\*\*, 014013 \(2011\)](#).
- [69] A. C. Aguilar, J. C. Cardona, M. N. Ferreira, and J. Papavassiliou, [Phys. Rev. \*\*D98\*\*, 014002 \(2018\)](#).
- [70] V. A. Miransky, [Dynamical symmetry breaking in quantum field theories](#) (World Scientific, 1994).
- [71] P. Maris, C. D. Roberts, and P. C. Tandy, [Phys. Lett. \*\*B420\*\*, 267 \(1998\)](#).
- [72] C. Itzykson and J. B. Zuber, *Quantum Field Theory*, International Series in Pure and Applied Physics (New York, USA: Mcgraw-Hill (1980) 705 p., 1980).
- [73] M. Mitter, J. M. Pawłowski, and N. Strodthoff, [Phys. Rev. \*\*D91\*\*, 054035 \(2015\)](#).
- [74] A. K. Cyrol, M. Mitter, J. M. Pawłowski, and N. Strodthoff, [Phys. Rev. \*\*D97\*\*, 054006 \(2018\)](#).
- [75] F. Ihssen, J. M. Pawłowski, F. R. Sattler, and N. Wink, [arXiv:2408.08413 \[hep-ph\] \(2024\)](#).
- [76] W. Celmaster and R. J. Gonsalves, [Phys. Rev. D \*\*20\*\*, 1420 \(1979\)](#).
- [77] J. Skullerud and A. Kizilersu, [J. High Energy Phys. \*\*2002\*\* \(09\), 013](#).
- [78] A. Kizilersü, O. Oliveira, P. J. Silva, J.-I. Skullerud, and A. Sternbeck, [Phys. Rev. D \*\*103\*\*, 114515 \(2021\)](#).

- [79] A. C. Aguilar, M. N. Ferreira, D. Ibáñez, and J. Papavassiliou, [Eur. Phys. J. C \*\*83\*\*, 967 \(2023\)](#).
- [80] A. I. Davydychev, P. Osland, and L. Saks, [Phys. Rev. \*\*D63\*\*, 014022 \(2001\)](#).
- [81] N. Brown and N. Dorey, [Mod. Phys. Lett. \*\*A6\*\*, 317 \(1991\)](#).
- [82] D. C. Curtis and M. R. Pennington, [Phys. Rev. D \*\*42\*\*, 4165 \(1990\)](#).
- [83] D. C. Curtis and M. R. Pennington, [Phys. Rev. D \*\*48\*\*, 4933 \(1993\)](#).
- [84] J. C. R. Bloch, [Phys. Rev. D \*\*64\*\*, 116011 \(2001\)](#).
- [85] J. C. R. Bloch, [Phys. Rev. D \*\*66\*\*, 034032 \(2002\)](#).
- [86] A. Kizilersu and M. Pennington, [Phys. Rev. \*\*D79\*\*, 125020 \(2009\)](#).
- [87] A. Ayala, A. Bashir, D. Binosi, M. Cristoforetti, and J. Rodriguez-Quintero, [Phys. Rev. \*\*D86\*\*, 074512 \(2012\)](#).
- [88] D. Binosi, C. D. Roberts, and J. Rodriguez-Quintero, [Phys. Rev. D \*\*95\*\*, 114009 \(2017\)](#).
- [89] G. Eichmann, [arXiv:2503.10397 \[hep-ph\] \(2025\)](#).
- [90] A. Blum, M. Q. Huber, M. Mitter, and L. von Smekal, [Phys. Rev. \*\*D89\*\*, 061703 \(2014\)](#).
- [91] G. Eichmann, R. Williams, R. Alkofer, and M. Vujanovic, [Phys. Rev. \*\*D89\*\*, 105014 \(2014\)](#).
- [92] A. C. Aguilar, M. N. Ferreira, J. Papavassiliou, and L. R. Santos, [Eur. Phys. J. C \*\*83\*\*, 549 \(2023\)](#).
- [93] F. Pinto-Gómez, F. De Soto, M. N. Ferreira, J. Papavassiliou, and J. Rodríguez-Quintero, [Phys. Lett. B \*\*838\*\*, 137737 \(2023\)](#).
- [94] F. Pinto-Gómez, F. De Soto, and J. Rodríguez-Quintero, [Phys. Rev. D \*\*110\*\*, 014005 \(2024\)](#).
- [95] A. Athenodorou, D. Binosi, P. Boucaud, F. De Soto, J. Papavassiliou, J. Rodriguez-Quintero, and S. Zafeiropoulos, [Phys. Lett. \*\*B761\*\*, 444 \(2016\)](#).
- [96] H. Sanchis-Alepuz and R. Williams, [Comput. Phys. Commun. \*\*232\*\*, 1 \(2018\)](#).
- [97] M. Q. Huber, [arXiv:2510.18960 \[hep-ph\] \(2025\)](#).
- [98] R. B. Lehoucq and D. C. Sorensen, [SIAM Journal on Matrix Analysis and Applications \*\*17\*\*, 789 \(1996\)](#), <https://doi.org/10.1137/S0895479895281484>.
- [99] R. B. Lehoucq, D. C. Sorensen, and C. Yang, [ARPACK Users' Guide](#) (Society for Industrial and Applied Mathematics, 1998) <https://epubs.siam.org/doi/pdf/10.1137/1.9780898719628>.
- [100] R. Alkofer, W. Detmold, C. S. Fischer, and P. Maris, [Phys. Rev. D \*\*70\*\*, 014014 \(2004\)](#).
- [101] G. Eichmann, A. Krassnigg, M. Schwinzerl, and R. Alkofer, [Annals Phys. \*\*323\*\*, 2505 \(2008\)](#).
- [102] A. Windisch, M. Q. Huber, and R. Alkofer, [Phys. Rev. D \*\*87\*\*, 065005 \(2013\)](#).



- [103] G. Eichmann, P. Duarte, M. T. Peña, and A. Stadler, [Phys. Rev. D \*\*100\*\*, 094001 \(2019\)](#).
- [104] C. S. Fischer and M. Q. Huber, [Phys. Rev. D \*\*102\*\*, 094005 \(2020\)](#).
- [105] M. Q. Huber, W. J. Kern, and R. Alkofer, [Phys. Rev. D \*\*107\*\*, 074026 \(2023\)](#).
- [106] J. Horak, J. M. Pawłowski, and N. Wink, [SciPost Phys. Core \*\*8\*\*, 048 \(2025\)](#).
- [107] D. C. Duarte, T. Frederico, W. de Paula, and E. Ydrefors, [Phys. Rev. D \*\*105\*\*, 114055 \(2022\)](#).
- [108] J. Braun *et al.*, [SciPost Phys. Core \*\*6\*\*, 061 \(2023\)](#).
- [109] G. Eichmann, A. Gómez, J. Horak, J. M. Pawłowski, J. Wessely, and N. Wink, [Phys. Rev. D \*\*109\*\*, 096024 \(2024\)](#).
- [110] J. Horak, F. Ihssen, J. M. Pawłowski, J. Wessely, and N. Wink, [Phys. Rev. D \*\*110\*\*, 056009 \(2024\)](#).
- [111] J. M. Pawłowski and J. Wessely, [Eur. Phys. J. C \*\*85\*\*, 970 \(2025\)](#).
- [112] C. S. Fischer, P. Watson, and W. Cassing, [Phys. Rev. D \*\*72\*\*, 094025 \(2005\)](#).
- [113] C. S. Fischer, D. Nickel, and R. Williams, [Eur. Phys. J. C \*\*60\*\*, 47 \(2009\)](#).
- [114] A. Krassnigg, [PoS \*\*CONFINEMENT8\*\*, 075 \(2008\)](#).